

SPECTRAL ESTIMATION FOR POINT PROCESSES AND RANDOM FIELDS

A PREPRINT

✉ J. P. GRAINGER^{*1}, ✉ T. A. RAJALA^{†2}, ✉ D. J. MURRELL^{‡3}, and ✉ S. C. OLHEDE^{§1}

¹Institute of Mathematics, École Polytechnique Fédérale de Lausanne, Station 8, 1015 Lausanne, Switzerland

²Natural Resources Institute Finland, 00790 Helsinki, Finland

³Research Department of Genetics, Evolution and Environment, Centre for Biodiversity and Environment Research, University College London, UK

September 27, 2024

ABSTRACT

Spatial variables can be observed in many different forms, such as regularly sampled random fields (lattice data), point processes, and randomly sampled spatial processes. Joint analysis of such collections of observations is clearly desirable, but complicated by the lack of an easily implementable analysis framework. It is well known that Fourier transforms provide such a framework, but its form has eluded data analysts. We formalize it by providing a multitaper analysis framework using coupled discrete and continuous data tapers, combined with the discrete Fourier transform for inference. Using this set of tools is important, as it forms the backbone for practical spectral analysis. In higher dimensions it is important not to be constrained to Cartesian product domains, and so we develop the methodology for spectral analysis using irregular domain data tapers, and the tapered discrete Fourier transform. We discuss its fast implementation, and the asymptotic as well as large finite domain properties. Estimators of partial association between different spatial processes are provided as are principled methods to determine their significance, and we demonstrate their practical utility on a large-scale ecological dataset.

Keywords Spatial point pattern · random field · spectral representation · spatial multitapering · coherence · partial coherence.

1 Introduction

Collections of spatial variables studied in geostatistics, ecology and other spatial sciences involve complex interactions between a variety of different components. Often we need to analyze data of different types, such as spatial point patterns, marked point patterns and realizations of random fields. We therefore need a common framework to allow all data types in our analysis. Spectral analysis provides a convenient way to construct notions of correlation and partial correlation between these different types of processes. In this paper, we develop methodology to estimate such quantities for any combination of point patterns, marked point patterns and realizations of random fields, when the processes may be recorded with differing sampling methods, and when the observational region is not necessarily rectangular, but common to all observed spatial variables. Existing methodology, with the exception of methodology for univariate Gaussian random fields (Andén and Romero, 2020), cannot handle arbitrary observational regions or different sampling mechanisms (including Rajala et al. 2023), and the existing spectral estimation methodology for marked point processes can be seen to be biased. All of these issues are resolved by the novel methodology that we propose in this paper.

^{*}jake.grainger@epfl.ch

[†]tuomas.rajala@iki.fi

[‡]d.murrell@ucl.ac.uk

[§]sofia.olhede@epfl.ch

Probabilistically, a spectral representation for general multivariate random measures has already been available for some time (Brillinger, 1972; Daley and Vere-Jones, 2003), providing the theoretical background for our work. However, statistical estimation of the spectral density matrix function for such processes has not been developed. Our introduction of multitapering is a necessary step to develop statistical methodology for the spectral analysis of multivariate spatial data. We show in simulations that the large sample theory developed in this paper is applicable to data which is similar to data of practical interest, on which we also illustrate our methodology. This enables us to use principled thresholds to determine significance, and gives confidence in the quality of the proposed methodology.

Although methodology for spectral estimation exists for spatial point processes (Bartlett, 1964; Diggle et al., 1987; Muggleston and Renshaw, 1996b,a; Rajala et al., 2023) and random fields (Bandyopadhyay and Lahiri, 2009; Matsuda and Yajima, 2009) separately, the extension to multivariate spatial data is more challenging. Kanaan et al. (2008) proposed an estimator for the cross-spectral density function between a random field and an unmarked point pattern, but this is limited to random fields which are sampled continuously in a rectangular region. Eckardt and Mateu (2019c) propose a periodogram when the random field is recorded on an integer grid within a rectangular domain, but do not study its properties or discuss smoothing or tapering. In reality, random fields can never be sampled continuously, and often we have multiple random fields recorded on different grids. Handling this is not trivial, and getting it wrong can result in substantial bias. We also want to consider marked point processes. A periodogram estimator has been proposed in the marked setting (Renshaw, 2002; Eckardt and Mateu, 2019b), however, this estimator is biased (see the Supplementary Material for details). Therefore, there are a number of outstanding issues which need to be resolved in order to develop a unified framework for spectral analysis of multivariate spatial data which can be used in practice.

Whilst Simons and Wang (2011); Andén and Romero (2020) consider spectral estimation for univariate Gaussian random fields on non-rectangular domains, performing such analysis in the case of multivariate random measures is more challenging. In particular, one first needs to construct continuous families of taper functions, in order to analyse the point processes, and then also build discrete families of taper sequences which are appropriate for each grid used to record the random fields, but that are related to the continuous tapers (otherwise estimates of cross statistics will be biased). We start from the discrete tapers of Simons and Wang (2011) and use these to generate continuous tapers, utilising the low wavenumber concentration already required to retain the same desirable properties. We then construct discrete taper sequences from the continuous tapers, again exploiting the low wavenumber concentration. As a result, we can combine all of these different kinds of data together, with no need for aggregation or interpolation, and requiring no additional tuning parameters beyond the single bandwidth parameter already used for multitaper estimation in the case of time series and random fields, (Walden, 2000). This results in methodology which neatly handles all of these additional complexities presented by the richer class of spatial processes.

In Section 4.1, we consider spatial data from a well known ecological study on Barro Colorado Island, Panama (Condit et al., 2019). One of the biological questions we consider concerns the relationship between two tree species and gradient of the terrain. One can see that there is some relationship, but it is not clear if this is due to both species preferring to grow on slopes (a purely abiotic cause), or if one species grows on slopes, and the other grows near to that species for some other biotic reason. Motivated by this question, we construct models for both cases which produce similar realisations to the observed spatial data, and use those in our simulation study. A realisation of each of the two models is shown in Fig. 1, where we can see the distinction between the two cases is far from obvious. Encouragingly, the partial coherence can distinguish between these two cases, and, our estimation technique can reliably recover this partial coherence, as we demonstrate in our simulation study.

In this paper, we provide a single unified multitaper framework for estimation of the spectra and cross-spectra of random fields, point processes and marked point processes. The methodology is discussed in detail, as is the implementation. We verify the properties of the proposed estimator through simulation studies, the first of their kind for spectral analysis of multivariate spatial data, and apply the methodology to forest ecology data from Barro Colorado Island. Several outstanding issues, long eluding the successful development of spectral analysis in this setting are resolved, including the extension to non-rectangular regions, the bias in the marked case, and handling different kinds of grid sampling. We then discuss using this framework to compute estimates of coherence and partial coherence between the different processes, with principled significance thresholds. We further demonstrate the promise of spectral analysis to summarize dependence in such complex systems, and provide methodology to perform inference.

2 Background

In order to discuss estimation, we first need to introduce the spectral density function for the various processes of interest. A point process is a random set of locations in some space, say \mathbb{R}^d , such that there are finitely many points within a given bounded region (Møller and Waagepetersen, 2003). A marked point process is a point process with additional information at each of the points, called a mark, which we shall take to be real-valued and non-negative. The

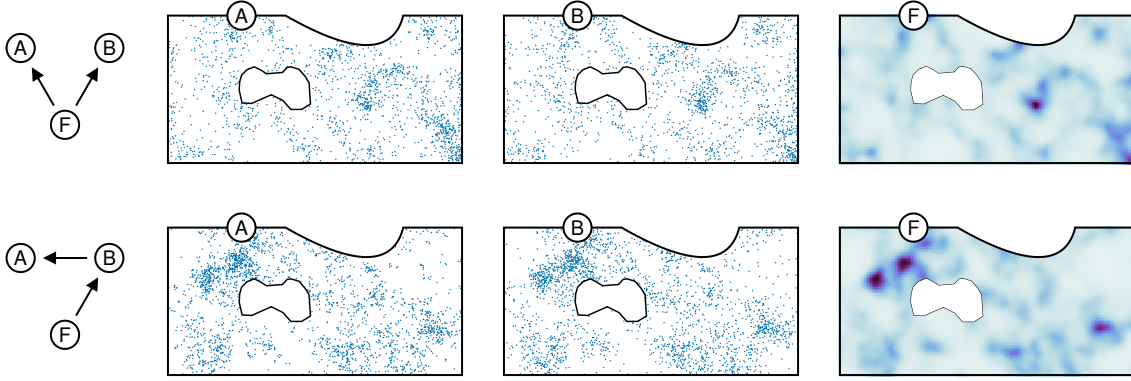


Figure 1: Example realisations of two spatial processes with different generating mechanisms. The spatial axes range from 0m to 1000m and 0m to 500m.

unmarked case is recovered by setting the distribution of the marks to be a point mass at 1. Let X be the set of random point locations, and $W(x)$ be the mark at location x . The mark-sum measure, or count measure in the unmarked case, (Daley and Vere-Jones, 2003) is

$$\xi(A) = \sum_{x \in X \cap A} W(x).$$

A random field is a random function, say Y , on \mathbb{R}^d (Adler, 2010). Assuming the random field is almost surely continuous and non-negative and has finite variance, we can define a random measure from the field by

$$\xi(A) = \int_A Y(u) du.$$

So random measures provide a unified framework in which to study these different spatial processes (Daley and Vere-Jones, 2003).

Assume that we have P such processes, and augment our previous notation by writing ξ_p for the p^{th} random measure. Assume that these processes are stationary, then there is a notation of spectral density matrix function for such multivariate random measures (Daley and Vere-Jones, 2003). From Chapter 8 of Daley and Vere-Jones (2003), for stationary multivariate random measures, the moment measures for $1 \leq p, q \leq P$

$$\begin{aligned} M_p(A) &= E \{ \xi_p(A) \} \\ M_{p,q}(A \times B) &= E \{ \xi_p(A) \xi_q(B) \} \end{aligned}$$

have reduced forms so that for any g a bounded measurable function of bounded support

$$\begin{aligned} M_p(A) &= \int_A \lambda_p du \\ \int_{\mathbb{R}^d} \int_{\mathbb{R}^d} g(x, y) M_{p,q}(dx \times dy) &= \int_{\mathbb{R}^d} \int_{\mathbb{R}^d} g(s + u, s) \ell(ds) \check{M}_{p,q}(du) \end{aligned}$$

where λ_p is the intensity if the p^{th} process is a simple point process, the mean if it is a random field, and the product of the mean mark and the intensity of the ground process if it is a marked point process (Illian et al., 2008, equation 5.1.19). The reduced covariance (signed) measure between the p^{th} and q^{th} process is given by

$$\check{C}_{p,q}(du) = \check{M}_{p,q}(du) - \lambda_p \lambda_q \ell(du).$$

Whilst they do not necessarily have densities, we will write a generalized density (which may have point masses) as $\check{c}_{p,q}$, which satisfies

$$\check{C}_{p,q}(A) = \int_A \check{c}_{p,q}(u) du.$$

If $p = q$ and the process in question is a simple point process with a reduced factorial moment density $\rho_{p,p}(u)$, then, writing $\delta(\cdot)$ for the Dirac delta function, we have

$$\check{c}_{p,p}(u) = \rho_{p,p}(u) - \lambda_p^2 + \lambda_p \delta(u)$$

which is referred to as the complete covariance function by Bartlett (1963), who first introduced the spectra of point processes. If the processes in question are both random fields, then

$$\check{c}_{p,q}(u) = \text{cov}(Y_p(u), Y_q(0)),$$

the usual autocovariance function. The notion of spectra exists in a more general form than the one given here, see Daley and Vere-Jones (2003), but we are interested in processes for which the spectral density function exists.

Assumption 1. *The reduced covariance measure $\check{C}_{p,q}$ is totally finite with a singular component comprised of finitely many point masses. In the case where both processes are random fields, the covariance density $\check{c}_{p,q}$ is a continuous function.*

If Assumption 1 holds, the (cross) spectral density function between the i^{th} and j^{th} processes exists and is defined as

$$f_{p,q}(k) = \int_{\mathbb{R}^d} \check{c}_{p,q}(u) e^{-2\pi i k u} du \quad k \in \mathbb{R}^d.$$

This definition corresponds with the usual notion of spectral density function from time series and random fields, as well as including the point process case as introduced by Bartlett (1963). However, in the marked case it should be noted that this differs slightly from the definition introduced by Renshaw (2002). In particular, they define the spectral density to be proportional to the Fourier transform of the reduced factorial moment density of the mark-sum measure, whilst we define it to be the Fourier transform of the reduced covariance measure. Importantly, this means we inherit all of the properties of the spectral density matrix function of multivariate random measures listed by Daley and Vere-Jones (2003), such as positive semi-definiteness etc., and setting the marks distribution to a point mass at 1 recovers the unmarked case. Call the matrix valued function $f(k) = [f_{p,q}(k)]_{1 \leq p,q \leq P}$ the spectral density matrix function of the processes at wavenumber $k \in \mathbb{R}^d$. This plays the role of a wavenumber domain covariance (Brillinger, 1972; Daley and Vere-Jones, 2003).

So far, we are constrained to random fields which are almost surely non-negative, however, this condition can be relaxed by viewing them as random-signed measures. Not all of the theory follows (such as the existence of moment measures), but spectra can be defined, see Daley and Vere-Jones (2003) for details. If these random measures do have reduced covariance measures satisfying Assumption 1, then we can also perform estimation with our framework (e.g. for many Gaussian processes).

3 Methodology

3.1 Multitapering

We aim to estimate $f(k)$ from a single realisation of the processes in question observed on some region $\mathcal{R} \subset \mathbb{R}^d$. We construct a form of multitapering, first developed for time series by Thomson (1982), due to its computational efficiency and very good leakage properties, which are often of great practical importance (Walden, 2000). By averaging over a family of tapered periodograms, which are asymptotically pairwise uncorrelated, one can obtain a consistent estimator for the periodogram. We will begin by assuming that we have recorded the random fields continuously in space (which of course is not possible), and then discuss the extension to sampled random fields in Section 3.2.

Definition 1. *Let $\{h_m : \mathbb{R}^d \rightarrow \mathbb{R}\}_{1 \leq m \leq M}$ be a family of $M \geq 1$ tapers. Denote the Fourier transform of a given taper h_m by*

$$H_m(k) = \int_{\mathbb{R}^d} h_m(s) e^{-2\pi i s \cdot k} ds, \quad k \in \mathbb{R}^d.$$

Assumption 2. *For a given region \mathcal{R} , the family of tapers $\{h_m\}_{1 \leq m \leq M}$ for some $M \in \mathbb{N}$ are chosen so that they are an orthonormal family of functions in L^2 which are supported on \mathcal{R} and satisfy $\|h_m\|_\infty < \infty$ and $H_m \in L^1$ for all $1 \leq m \leq M$.*

The m^{th} tapered Fourier transform of the p^{th} process is defined as

$$J_{p;m}(k) = \int_{\mathbb{R}^d} h_m(s) e^{-2\pi i s \cdot k} \xi_p(ds) - \hat{\lambda}_p H_m(k),$$

where $\hat{\lambda}_p$ is an estimate of the intensity of the random measure. For a marked point process, recalling that X_p denotes the locations of the points and $W_p(x)$ denotes the mark at $x \in X_p$

$$J_{p;m}(k) = \sum_{x \in X_p} h_m(x) W_p(x) e^{-2\pi i x \cdot k} - \hat{\lambda}_p H_m(k),$$

whilst for random fields, recalling that Y_p denotes the random field

$$J_{p;m}(k) = \int_{\mathbb{R}^d} h_m(s) \{Y_p(s) - \hat{\lambda}_p\} e^{-2\pi i s \cdot k} ds.$$

The tapered periodogram and multitaper spectral estimate between processes p and q are

$$I_{p,q;m}(k) = J_{p;m}(k) \overline{J_{q;m}(k)}, \quad \hat{f}_{p,q}(k) = \frac{1}{M} \sum_{m=1}^M I_{p,q;m}(k), \quad (1)$$

for $k \in \mathbb{R}^d$, respectively. As for time series (Percival and Walden, 1993), the expectation of the periodogram can be expressed as a convolution of the spectral density function with $|H_m(\cdot)|^2$, which is called the spectral window. In particular, as a special case of Proposition 2, if we replace the intensity estimates with the true intensities

$$E \{I_{p,q;m}(k)\} = \int_{\mathbb{R}^d} |H_m(k - k')|^2 f_{p,q}(k') dk',$$

for $1 \leq p, q \leq P$ and $1 \leq m \leq M$ and for all $k \in \mathbb{R}^d$. Heuristically, if the spectral window $|H_m(\cdot)|^2$ behaves like a Dirac delta function, the tapered periodogram is unbiased. The specific shape of the spectral window determines the properties of the periodogram and, by extension, multitaper estimator (Percival and Walden, 1993). Therefore, the choice of tapers is crucial for performance. In particular, the spectral window should be as concentrated as possible within a region around wavenumber zero (Slepian and Pollak, 1961; Thomson, 1982; Simons and Wang, 2011).

3.2 Sampled random fields

We have defined a collection of tapers for processes sampled continuously in space. However, we typically observe random fields sampled on a regular grid. Define a grid $\mathcal{G} = \{z \circ \Delta + v \mid z \in \mathbb{Z}^d\}$ where $\Delta \in \mathbb{R}_{>0}^d$ denotes the sampling interval and $v \in \mathbb{R}^d$ denotes the offset of the grid, with \circ being the Hadamard product. We may require more than one grid, and will augment the notation when necessary. In order to understand the effect of sampling, it is useful to introduce a grid sampled function. For some function g , let the grid sampled function $g^{(\mathcal{G})}$ be

$$g^{(\mathcal{G})}(s) = g(s) \left(\prod_{j=1}^d \Delta_j \right) \sum_{z \in \mathcal{G}} \delta(s - z),$$

for $s \in \mathbb{R}^d$, where $\delta(\cdot)$ is the Dirac delta function as before and Δ_j denotes the j^{th} element of Δ . So we allow different sampling periods in different dimensions. Now by definition, the Fourier transform of such a discrete taper is

$$G^{(\mathcal{G})}(k) = \int_{\mathbb{R}^d} g^{(\mathcal{G})}(u) e^{-2\pi i u \cdot k} du = \left(\prod_{j=1}^d \Delta_j \right) \sum_{u \in \mathcal{G}} g(u) e^{-2\pi i u \cdot k},$$

for $k \in \mathbb{R}^d$, which is periodic on $K_\Delta = \prod_{j=1}^d [-1/2\Delta_j, 1/2\Delta_j]$.

For a random field sampled on a grid, we define the tapered Fourier transform as

$$\begin{aligned} J_{p;m}(k) &= \int_{\mathbb{R}^d} h_m^{(\mathcal{G})}(u) e^{-2\pi i u \cdot k} \xi_p(du) - \hat{\lambda}_p H_m^{(\mathcal{G})}(k) \\ &= \left(\prod_{j=1}^d \Delta_j \right) \sum_{s \in \mathcal{G}} h_m(s) \{Y(s) - \hat{\lambda}_p\} e^{-2\pi i s \cdot k} ds. \end{aligned}$$

Assume that the p^{th} process has been sampled on the grid \mathcal{G} , but the q^{th} has been sampled continuously (e.g. it is a point pattern), then as another special case of Proposition 2, we have

$$E \{I_{p,q;m}(k)\} = \int_{\mathbb{R}^d} H_m^{(\mathcal{G})}(k - k') \overline{H_m(k - k')} f_{p,q}(k') dk'.$$

Thus heuristically, if $H_m^{(\mathcal{G})}$ behaves sufficiently similarly to H_m , then we will also obtain good estimates (in terms of bias). In fact, H_m and $H_m^{(\mathcal{G})}$ are related by the aliasing relation (Percival and Walden, 1993, for example), a variant of which is given by the following proposition.

Proposition 1. *Consider sampling one of our continuous tapers, then given Assumption 2,*

$$H_m^{(\mathcal{G})}(k) = \sum_{z \in \mathbb{Z}^d} H_m(k + z \odot \Delta) e^{-2\pi i v \cdot (z \odot \Delta)}, \quad \forall k \in \mathbb{R}^d,$$

where \odot denotes element-wise (Hadamard) division.

If we further assume that H_m is supported on some region $\mathcal{K} \subseteq K_\Delta$, then for $k \in K_\Delta$,

$$H_m^{(\mathcal{G})}(k + z' \odot \Delta) = H_m(k) e^{2\pi i v \cdot (z' \odot \Delta)}, \quad \forall z' \in \mathbb{Z}^d.$$

Furthermore, in this case $H_m^{(\mathcal{G})}(k) \overline{H_m^{(\mathcal{G})}(k)} = |H_m(k)|^2$ because $H_m(k + z' \odot \Delta) = 0$ for $z' \neq 0$. Whilst we cannot have a taper be supported on a bounded region in wavenumber, because the taper is supported on a bounded region in space, we can construct tapers by maximizing concentration in wavenumber (Slepian and Pollak, 1961; Slepian, 1983; Simons and Wang, 2011). Asymptotics for multitapering essentially require that H_m is increasingly concentrated within some shrinking bandwidth of zero. Therefore, H_m is concentrated within the Nyquist box for an appropriately small bandwidth, and thus the above argument can be applied (made formal in the proof of Theorem 1). For a given finite region, using the methodology of Simons and Wang (2011) we can construct tapers which are (approximately) optimally concentrated within such a region.

We will generalize our notation so that for any $1 \leq p \leq P$, the tapered Fourier transform for the p^{th} process is

$$J_{p;m}(k) = \int_{\mathbb{R}^d} h_{p;m}(u) e^{-2\pi i u \cdot k} \xi_p(\mathrm{d}u) - \hat{\lambda}_p H_{p;m}(k)$$

where $h_{p;m}$ is the appropriate taper for the given sampling regime, i.e. if the p^{th} process is a (marked) point process $h_{p;m} = h_m$ and if the p^{th} process is a random field sampled on the grid \mathcal{G}_p then $h_{p;m} = h_m^{(\mathcal{G}_p)}$. For a given m , the taper is always the same for two point processes, but for random fields will depend on the sampling grid. Though these tapers are closely related as we merely subsample the base taper (with appropriate rescaling). The periodogram and multitaper spectral estimate are as defined in (1).

Unless specified otherwise, we shall assume for simplicity that the intensity/mean λ_p is known, which we refer to as the “oracle case”. Estimating the intensity has a negligible effect, except near zero wavenumber. However, the finite sample equations become more complicated, and so we consider the oracle case here, and the non-oracle case is discussed in the Supplementary Material. We can now obtain a general expression for the effect of the tapers on the periodogram including the grid sampling.

Proposition 2 (Expectation of the periodogram). *Given the processes satisfy Assumption 1 and the tapers satisfy Assumption 2, the expectation of the periodogram is*

$$E \{ I_{p,q;m}(k) \} = \int_{\mathbb{R}^d} H_{p;m}(k - k') \overline{H_{q;m}(k - k')} f_{p,q}(k') \mathrm{d}k',$$

for all $m \in \mathbb{N}$, $k \in \mathbb{R}^d$.

This generalizes the standard result for multivariate time series (Walden, 2000), random fields (Guillaumin et al., 2022) and univariate point processes (Rajala et al., 2023). Since the expectation is a convolution between the true spectral density function and a property of the taper, we can control bias by constraining the behaviour of the taper.

In practice, we will use the methodology of Simons and Wang (2011) to construct the tapers on a discretized region, and then construct continuous tapers by linearly interpolating between the grid points. Specific details of the taper construction and effect of the linear interpolation are given in the Supplementary Material, but intuitively as the tapers have Fourier transforms focused at low wavenumber, they have little short scale variability. The computation of the tapered Fourier transforms in the case of random fields sampled on a regular grid can easily be achieved with Fast Fourier Transforms (FFTs) (Cooley and Tukey, 1965), as is well known. In the case of point patterns, this can also be achieved with the more recently developed Non-Uniform Fast Fourier Transforms (NUFFTs), the properties of which were studied by Dutt and Rokhlin (1993). We use the NUFFT implementation from Barnett et al. (2019).

3.3 Asymptotic framework

We consider the properties of our estimator under growing domain asymptotics. In particular, consider a sequence of regions $\{\mathcal{R}_n\}_{n \in \mathbb{N}}$ which satisfy the following assumption.

Assumption 3. Assume that for all $n \in \mathbb{N}$, $\mathcal{R}_n \subset \mathcal{R}_{n+1}$ and there exists some box such that $\prod_{j=1}^d [a_{j;n}, b_{j;n}] \subseteq \mathcal{R}_n$. Furthermore, that $\ell(\bigcup_{n=1}^{\infty} \mathcal{R}_n) = \infty$.

A box within a region is sufficient to guarantee the existence of a family of tapers for that region, as we can always take outer products of one-dimensional continuous tapers, such as the minimum bias tapers of Riedel and Sidorenko (1995). We augment the previous notation to add a second subscript following the taper index, e.g. the tapered Fourier transform with the m^{th} taper corresponding to the n^{th} region is $J_{p;m,n}$.

To obtain a consistent estimator, we need to take the number of tapers to infinity as the region grows. However, for now it is useful to consider the effect of growing domain for a fixed number of tapers, as in Lii and Rosenblatt (2008) and Astfalck et al. (2024). We give results for a growing number of tapers in the Appendix. It is useful to make the relation between the Fourier transform of the base taper, $H_{m,n}$, and the sampled taper, $H_{p;m,n}$, explicit for all processes in question.

Definition 2. For continuously sampled processes and random fields sampled on a grid, we can write the Fourier transform of the taper used in the transform in the form

$$H_{p;m,n}(k) = \sum_{\psi \in \Psi_p} H_{m,n}(k + \psi) w_p(\psi),$$

where for a process sampled on a grid \mathcal{G}_p we have $\Psi_p = \{z \odot \Delta_p \mid z \in \mathbb{Z}^d\}$ and $w_p(\psi) = e^{-2\pi i v_p \cdot \psi}$ whilst for a continuously sampled process we have $\Psi_p = \{0\}$ and $w_p(\psi) = 1$.

Here the set Ψ_p describes the periodicity resulting from grid sampling, whilst the function w_p describes the phase shift caused by the grid not being centered at zero.

Definition 3. Let the aliased spectral density function be

$$\tilde{f}_{p,q}(k) = \sum_{\psi \in \Psi_p \cap \Psi_q} f_{p,q}(k + \psi) w_p(\psi) \overline{w_q(\psi)}, \quad k \in \mathbb{R}^d.$$

Regardless of sampling mechanism, $0 \in \Psi_p \cap \Psi_q$, and aliasing is only present if $\Psi_p \cap \Psi_q \neq \{0\}$. In particular, if one of the processes is sampled continuously in space then there is no aliasing. If both processes are sampled on grids which are the same, then we have the usual aliasing relation, as in Percival and Walden (1993). If the processes are sampled on different grids with the same offset ($v_p = v_q$), then the aliasing relation is more complicated, but there will be fewer wrapped wavenumbers. If the offsets are different then we get a phase shift in the wrapped terms (those involving $f_{p,q}(k + \psi)$ when $\psi \neq 0$). The contribution from the cross-spectral density function at the wavenumber of interest is not effected by this phase shift. If the process in question had a spectral density function which was bandlimited within the Nyquist box of the smallest grid, then there would be no bias, in particular the starting point of the grid doesn't matter.

Assumption 4. For each n , the family of tapers $\{h_{m,n}\}_{1 \leq m \leq M}$ satisfies the conditions of Assumption 2, and each taper is asymptotically concentrated so that for all $m \in \mathbb{N}$,

$$\int_{B_{b_n}(0)} |H_{m,n}(k)|^2 dk \rightarrow 1,$$

as $n \rightarrow \infty$, where $b_n \rightarrow 0$ as $n \rightarrow \infty$. Here b_n is called the bandwidth of the taper and $B_r(x)$ is the ball of radius r centred at x .

Theorem 1 (Asymptotic bias of the periodogram). Given Assumption 1 and 4, we have for any $k \in \mathbb{R}^d$

$$E \{I_{p,q;m,n}(k)\} \rightarrow \tilde{f}_{p,q}(k)$$

for all m , as $n \rightarrow \infty$.

Theorem 1 shows that the periodogram is asymptotically unbiased, up to aliasing effects which are unavoidable (unless we have access to the sampling mechanism and can do some preprocessing). Importantly, in the case where at least one of the processes is not sampled on a grid, the periodogram is asymptotically unbiased. This includes the case of marked point processes, meaning that we have resolved the bias present in the current state-of-the-art estimator.

Theorem 2 (Asymptotic normality of the tapered Fourier transforms). Given that Assumptions 1, 4, A1 and A2 hold, and $k \in \mathbb{R}^d$ is such that $2k \notin \bigcup_{p=1}^P \Psi_p$, let $J_{m,n}(k) = [J_{p;m,n}(k)]_{1 \leq p \leq P}$ then

$$J_{m,n}(k) \xrightarrow{d} \mathcal{CN}(0, \tilde{f}(k), 0)$$

as $n \rightarrow \infty$, where $CN(\mu, S, R)$ is a complex normal vector with mean μ , covariance S and relation R . In addition, for any two distinct m, m' , the vectors $J_{m,n}(k)$ and $J_{m',n}(k)$ are asymptotically independent. As a result, the matrix $J_n(k) = [J_{m,n}(k)^T]_{1 \leq m \leq M}$ is asymptotically complex normal with uncorrelated rows. Furthermore, if $k, k' \in \mathbb{R}^d$, such that $2k, 2k', k - k' \notin \bigcup_{p=1}^P \Psi_p$, then $J_n(k)$ and $J_n(k')$ are also asymptotically independent.

3.4 Magnitude coherence, group delay and magnitude partial coherence

Whilst the spectral density matrix function plays the role of a wavenumber domain cross-process covariance, we are also interested in correlation and partial correlation. Because the wavenumber domain process is complex-valued, its covariance, called complex coherence, is also complex-valued. Therefore, it is common to consider the absolute value of this correlation, magnitude coherence, and the sign, group delay (Carter, 1987), defined for $k \in \mathbb{R}^d$ by

$$r_{p,q}(k) = \frac{|f_{p,q}(k)|}{\{f_{p,p}(k)f_{q,q}(k)\}^{1/2}}, \quad \theta_{p,q}(k) = \arg f_{p,q}(k), \quad (2)$$

respectively. We write $\tilde{r}_{p,q}$ and $\tilde{\theta}_{p,q}$ for the aliased versions, substituting \tilde{f} for f in (2). Define $\mathcal{V} = \{1, \dots, P\}$ and $\mathcal{V}_{p,q} = \mathcal{V} \setminus \{p, q\}$. As with partial correlation, the magnitude partial coherence and partial group delay for $k \in \mathbb{R}^d$ are

$$r_{p,q|\mathcal{V}_{p,q}}(k) = \frac{|f_{p,q|\mathcal{V}_{p,q}}(k)|}{\{f_{p,p|\mathcal{V}_{p,q}}(k)f_{q,q|\mathcal{V}_{p,q}}(k)\}^{1/2}}, \quad \theta_{p,q|\mathcal{V}_{p,q}}(k) = \arg f_{p,q|\mathcal{V}_{p,q}}(k),$$

respectively (Dahlhaus, 2000; Eckardt and Mateu, 2019b), where $f_{p,q|\mathcal{V}_{p,q}}$ is the cross-spectral density function of two residual processes formed by producing the best linear prediction of ξ_p and ξ_q from the other processes $\{\xi_r \mid r \in \mathcal{V}_{p,q}\}$. More details can be found in Dahlhaus (2000) and Eckardt and Mateu (2019b), but importantly the magnitude partial coherence (and group delay) can be computed efficiently by inverting the spectral matrix and making appropriate transformations (Dahlhaus, 2000).

As usual for spectral estimation, we use a plug-in estimator for the magnitude coherence, group delay and their partial counterparts, though of course this requires the estimated spectral density matrix at a given frequency is invertible. So we need to have more tapers than processes, a necessary but not sufficient condition (Walden, 2000). In particular, we cannot use the periodogram as a plug-in estimator for the magnitude partial coherence as the periodogram is not invertible (Walden, 2000).

The probability density function of the absolute value of the sample correlation of a bivariate complex proper normal random vector with true absolute correlation ρ and number of observations N is

$$f(r; \rho, N) = 2(N-1)(1-\rho^2)^N r(1-r^2)^{N-2} {}_2F_1(N, N, 1; \rho^2 r^2) \quad (3)$$

if $0 < r < 1$ and zero otherwise (Miller, 1980). Provided the assumptions of Theorem 2 hold, the matrix $J_n(k)$ is asymptotically complex normal. Therefore, the plug in estimator for $r_{p,q}$, which is the absolute value of the sample correlation of the matrix $J_n(k)$, has an asymptotic distribution with probability density function given by (3), with $\rho = \tilde{r}_{p,q}$ and $N = M$, as in the case of segment averaging (Goodman, 1957; Carter et al., 1973).

The plug-in estimator for the magnitude partial coherence is the sample partial correlation of $J_n(k)$ (with known zero mean). This partial correlation is the sample correlation of the residuals of the regressions of $J_p(k)$ and $J_q(k)$ with $\{J_r(k) \mid r \in \mathcal{V}_{p,q}\}$ (Whittaker, 2009). If the number of tapers M is small, this approximation may be poor, however, in the spatial setting the number of tapers is typically large and thus this approximation performs well (we examine this in the Supplementary Material).

4 Simulations and applications

4.1 Application to BCI data

The Barro Colorado Island study records the locations of all of the individual trees of at least 10mm in trunk diameter within a 1000 by 500 metre rectangle of tropical rainforest, along with other useful measurements, such as the diameter and species of each individual tree (Condit et al., 2019). This monitoring was first performed in 1982 and has been repeated every five years since 1985. In addition, records of the elevation and gradient of the terrain, as well as the concentration of various soil chemicals, are available on regular grids. Whilst the study records data on a rectangular domain, it is known that the forest is not homogeneous. In particular, there is a region near the northern border of the plot known to consist of a much younger forest dominated by the pioneer tree species *Gustavia superba* (Hubbell and Foster, 1983, 1986), which we therefore remove from all of our analyses to make homogeneity a more reasonable

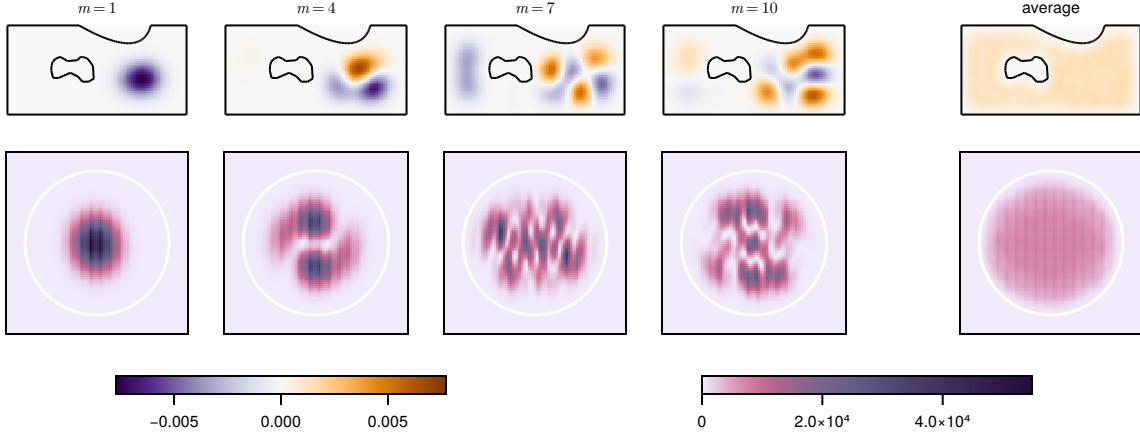


Figure 2: The a subset of four of the tapers and the total average absolute taper for the region excluding the swamp (top), and the corresponding spectral windows (bottom). The spatial data has axes 0 to 1000 and 0 to 500, and the wavenumber domain plots range from -0.01 to 0.01 in each dimension.

assumption. In addition, there is also a swamp region in the centre of the plot where the soil has much higher moisture content and the associated flora is more typical of a riparian habitat (Harms et al., 2001). For some species it may be appropriate to remove this region, and thus we consider the effect of such a removal in our analysis. Whilst the proposed methodology assumes homogeneity, this is homogeneity of the collection of processes as a whole, meaning that any one process may look very inhomogeneous, e.g. it could be conditionally inhomogeneous on another process (as with the log-Gaussian Cox process examples in Section 4.2).

A subset of the tapers we use when the swamp is excluded is shown in Fig. 2. Whilst any given taper heavily upweights a certain region of the domain, the total weight is assigned fairly uniformly across the spatial domain. Similarly, in the wavenumber domain we see that the spectral windows are concentrated on different regions within the bandwidth of zero (denoted by the white circle), but that on aggregate they cover this low wavenumber region evenly. This points to the major benefit of multitapering, as if we were to use a single taper and kernel smooth the resultant periodogram, we would be focusing on a small part of the observational region. To understand the final properties of the estimator, we would then need to jointly understand the kernel smoothing and tapering, which quickly becomes opaque for a complicated region. In contrast, multitaper estimation makes this easy and transparent, and avoids additional integral approximations which would be required for the kernel smoother, as in Yang and Guan (2024).

We will consider two different subsets of the available point patterns and random fields in this analysis. In each case, we will consider the magnitude coherence and magnitude partial coherence between the processes, but it is also useful to consider their signs (group delay and partial group delay) to understand if the processes are positively or negatively correlated (or something between as the correlation is complex). To display both group delay and magnitude coherence would require twice as many figures, and it can be difficult in the spatial context to keep track of the visualization across these figures (often one ends up just trying to see if the group delay at a significant wavenumber is closer to 0 or π). To have a group delay which is not 0 or π , the processes must be anisotropic. If the processes are isotropic, then it would be enough to visualize only these two cases (which correspond to a positive and negative correlation respectively). Such strong anisotropy is unlikely in our case (especially in the partial case as this accounts for covariates), and looking at the group delay and partial group delay, we see that for wavenumbers with large magnitude (partial) coherence they are close to 0 or π (see the Supplementary Material). Therefore, for visualization purposes we assign a positive sign if the (partial) group delay is closer to 0 than π and a negative sign otherwise, which we call signed (partial) coherence. Additionally, we only display the signed coherence and signed partial coherence when the magnitude exceeds a threshold chosen using the distribution in (3) and a Bonferroni correction (Bonferroni, 1936) at a 0.05 significance level. In particular, we correct as if we perform $K_n P(P-1)/2$ tests, where K_n are the approximate number of uncorrelated wavenumbers (spaced two bandwidths apart). We display more than K_n wavenumbers for visualization purposes, but threshold based on K_n . Basing the correction on the number of displayed wavenumbers would be overly conservative because estimates are correlated when they correspond to wavenumbers within two bandwidths of each other.

In our first analysis, we consider the two species *Beilschmiedia towarensis* and *Poulsenia armata*, because they are known to have a relation to the gradient of the terrain (Harms et al., 2001; Flüge et al., 2014), though these studies

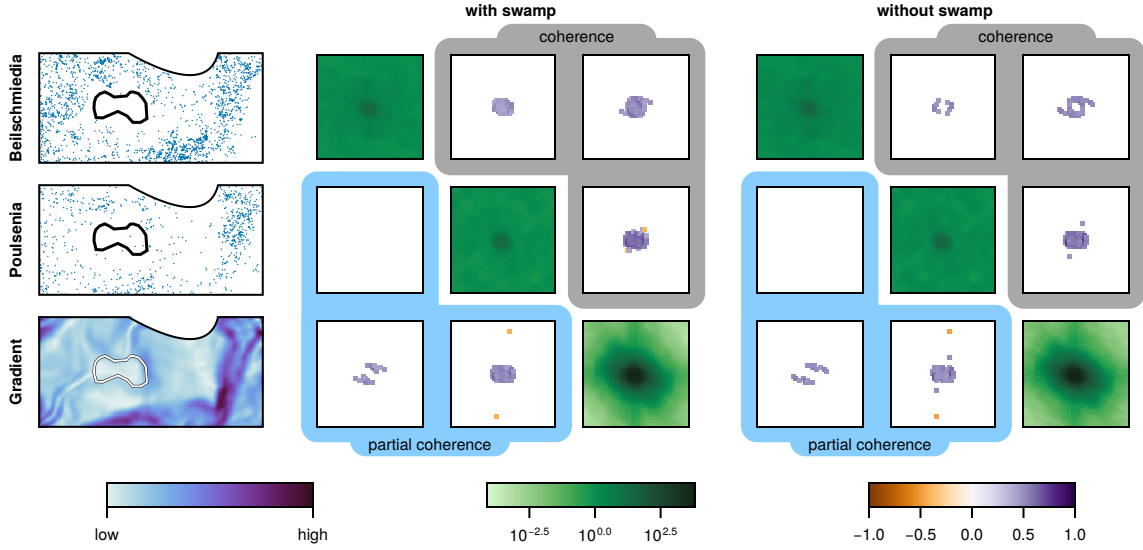


Figure 3: Analysis *Beilschmiedia towarensis*, *Poulsenia armata* and the gradient of the terrain. The spatial data has axes 0 to 1000 and 0 to 500, and the wavenumber domain plots show both k_1 and k_2 ranging from -0.05 to 0.05. Colorbars indicate from left to right, the value of the field from low to high, the value of the log standardized marginal spectra and the value of the signed coherence and signed partial coherence.

did not consider the possibility of species-species interaction as an alternative explanation. We use the 2015 (most recent published) census of the BCI data (Condit et al., 2019), and the gradient data is taken from the R package `spatstat` v3.0-1 (Baddeley et al., 2015). The locations of *Beilschmiedia towarensis* and *Poulsenia armata*, as well as the gradient of the terrain are displayed in the left column of Fig. 3 (the internal border is the swamp region). Estimated spectral matrices with and without the swamp are shown on the centre and right in Fig. 3, respectively. We show the log of the marginal spectral density function on the diagonal, signed coherence in the upper triangle and signed partial coherence in the lower triangle.

There is strong signed coherence between all pairs of processes considered. However, whilst there is still signed partial coherence between the gradient and each of the two species, there is no signed partial coherence between the two species, suggesting that the inclusion of gradient is enough to explain their correlation. That is, the prevalence of the two species is strongly dependent on the gradient, but they do not strongly impact each other. In addition, we see that the same effects are present if the swamp region is removed, but the signed coherence and signed partial coherence are slightly weaker in this case. This suggests that indeed it is affinity for slopes which drives *Beilschmiedia towarensis* and *Poulsenia armata* to grow near one another, and not some other biological reason.

Zemunik et al. (2020) considered the effect of Manganese and Phosphorus on four different species which are present in the BCI data, performing both experiments on seedlings and analysis on the BCI data. Zemunik et al. (2020) found that the concentration of Manganese and Phosphorus had a positive effect on the growth of *Tabebuia rosea* in seedlings, but their analysis of the BCI data found a slightly negative relation to Manganese, which one would expect as high concentrations of heavy metals are thought to be toxic to plants (Foy et al., 1978). We quantify the association between the concentration of Manganese and Phosphorus and the growth of *Tabebuia rosea* in the BCI data, using growth data computed by Zemunik et al. (2020) (which is individual growth from the 2005 to 2010 census).

Figure 4 shows that removing the swamp has a substantial effect on our analysis. In particular, if we include points within the swamp, we find a negative signed coherence and signed partial coherence between the concentration of Manganese and the growth of *Tabebuia rosea*, but a positive signed coherence and signed partial coherence between the concentration of Phosphorus and the growth of *Tabebuia rosea*. However, if we remove the swamp, we find that almost all signed coherence and signed partial coherence between *Tabebuia rosea* and the two chemicals has gone. In this case, it is not entirely clear if the swamp should or should not be included. If the swamp has no biological effect then we are substantially biasing the results because the swamp corresponds to a substantial region with low concentration of Manganese and high concentration of Phosphorus, and because removing the swamp substantially reduces the sample size for *Tabebuia rosea*. However, our methodology can include such complex region shapes, enabling easy

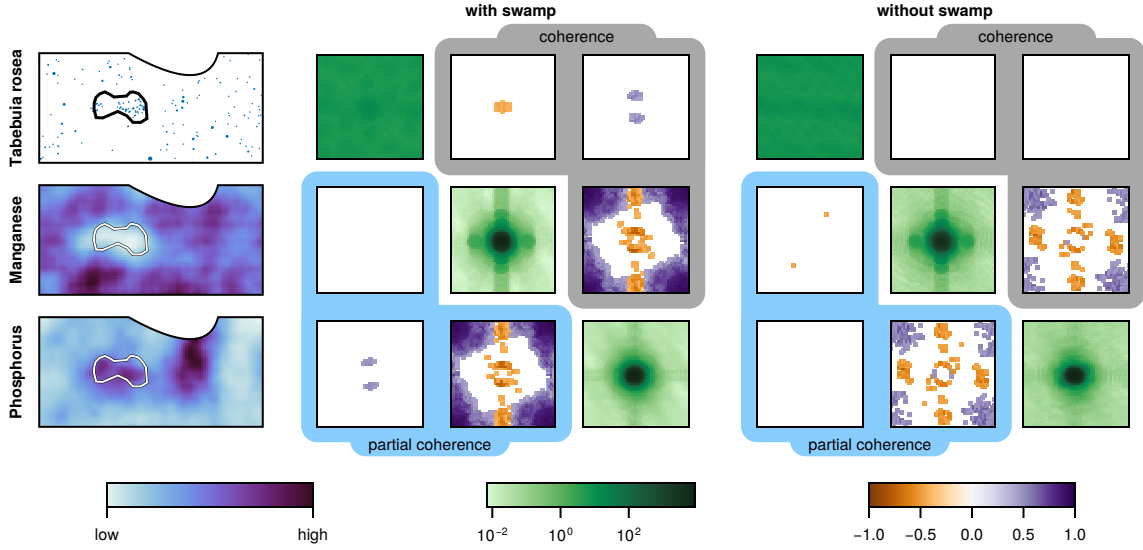


Figure 4: Analysis of the growth of *Tabebuia rosea* and the level of Manganese and Phosphorus in the soil. The layout is as in Fig. 3.

exploration of such hypotheses. With regards to the signed coherence between the two soil chemicals, there is a clear low wavenumber negative signed coherence as we would expect, but also high wavenumber positive signed coherence. This high wavenumber signed coherence is likely a spurious result of the interpolation used to produce the soil chemical maps, however, it will not have an effect on the low wavenumber region in which we are interested, as the signed partial coherence is computed at each wavenumber individually.

In conclusion, we have shown that our proposed methodology can be used to analyze the relation between different processes in a complex spatial setting. In particular, we saw in the first example that signed partial coherence is able to conveniently account for the confounding effect of the gradient on the two species, whilst in the second example we saw that the inclusion of the swamp region could have a substantial effect on the results, and therefore it is important that we can perform analysis on such regions, something which existing wavenumber domain methodology does not allow. This underscores the utility of wavenumber domain analysis.

4.2 Simulation study

In order to investigate the performance of our proposed methodology, we will consider a simulation study designed to be similar to some of the previous processes. In particular, motivated by the gradient example presented in Fig. 3, we will consider a simulation study with two point processes ξ_1 , ξ_2 and a random field ξ_3 . We consider three possible forms of interactions:

- Model 1: a null case, with marginal dependence but no cross-process dependence.
- Model 2: ξ_3 causes clustering within each of ξ_1 and ξ_2 independently.
- Model 3: ξ_3 causes clustering with ξ_2 , which subsequently causes clustering within ξ_1 .

Such dependence is achieved by a mixture of log-Gaussian Cox process (Møller et al., 1998) and cluster processes (Neyman and Scott, 1972) (see the Supplementary Material for specific details). It is not clear which underlying structure is correct from the spatial data alone (see Fig. 1 for examples of models 2 and 3), however, the spectral matrix is able to recover this structure.

For the simulation, we will consider the magnitude coherence and magnitude partial coherence between the processes, and compare the results to the true magnitude coherence and magnitude partial coherence (we omit the signed part as we are evaluating the choice of threshold in this simulation study). In particular, we will compare the simulated distributions to the asymptotic distributions given in (3). In these simulations, we use the region from the Barro Colorado Island data with the swamp removed (we give the equivalent results for the swamp included in the Supplementary Material).

For each case, we generate 1000 replications, and compute estimates of the spectral density matrix function. It is not possible to visualize all of the results, so we show a subset. In particular, we focus on two wavenumbers which illustrate different areas of the spectrum. The first is at a low wavenumber on the slope (so we expect smoothing effects to degrade the quality of the approximation), the third is at a high wavenumber, exploring the effects in the tails. At each of these wavenumbers, we show the empirical and asymptotic distributions of magnitude coherence and magnitude partial coherence between the point processes (processes 1 and 2) and between one of the point processes and the field (processes 2 and 3). The true models and simulation results are displayed in Fig. 5.

For model 1 (the null model), the empirical distribution of the magnitude coherence and magnitude partial coherence are as expected, the exception being wavenumber zero, where (as expected) it is not appropriate to use the asymptotic distribution.

In models 2 and 3, the asymptotic distributions begin to break down in some of the non-null cases. We do not expect the asymptotic distribution to be perfect in this case, and in these cases we would still detect the effect as being significant when compared to the null asymptotic distribution. In the null cases, the approximation is better, though we do see slightly larger values than expected in both the estimated magnitude coherence and magnitude partial coherence.

Peaks in coherence at non-zero wavenumbers would correspond to periodic patterns such as grids in the observed point pattern (as opposed to lumps in coherence centred at zero). Biologically we do not expect oscillatory behaviour in the locations of trees unless the forest is managed. In the case where some isolated “specks” of signed (partial) coherence are observed, this is likely due to the finite sample distribution of the signed (partial) coherence differing slightly from the asymptotic distribution in these cases. Based on this domain knowledge, one could then choose to discount these interactions as spurious. Indeed, this occurs in places in both Fig. 3 and Fig. 4. Thus it is important to look at the signed partial coherence, and consider the meaning of wavenumber, as simply applying a test across all wavenumbers could lead to spurious results in such cases.

Acknowledgement

Sofia Olhede would like to thank the European Research Council under Grant CoG 2015-682172NETS, within the Seventh European Union Framework Program.

A Additional assumptions and results

Let M_n be the number of available tapers for the region \mathcal{R}_n . For stating asymptotic results, it is convenient to have a sequence of tapers for each m , $\{h_{m,n}\}_{n \in \mathbb{N}}$. Since this is only relevant for the asymptotics, we assume that for all n , if $m > M_n$ then $h_{m,n}(s) = 0$ for all $s \in \mathbb{R}^d$.

Assumption A1. Let $\check{C}_{p_1, \dots, p_r}$ be the r^{th} cumulant measure of the processes $\xi_{p_1}, \dots, \xi_{p_r}$, and write $\check{c}_{p_1, \dots, p_r}$ for the corresponding density (in the generalized function sense). We require that for all $r \in \mathbb{N}$ and $p_1, \dots, p_r \in \{1, \dots, P\}$,

$$\int_{\mathbb{R}^d} \cdots \int_{\mathbb{R}^d} |\check{c}_{p_1, \dots, p_r}(u_1, \dots, u_{r-1})| du_1 \cdots du_{r-1} < \infty$$

and is continuous in the arguments corresponding to lags between random fields.

Assumption A2. For all $m \in \mathbb{N}$, $\|H_{m,n}\|_1 \rightarrow 0$ as $n \rightarrow \infty$.

Proposition A1. If Assumptions 1, 4, A1 (for $r = 4$) and A2 hold, and $M_n \rightarrow \infty$ and $n \rightarrow \infty$ then

$$\text{var} \left\{ \hat{f}_{p,q;n}(k) \right\} \rightarrow 0$$

as $n \rightarrow \infty$ for any $k \in \mathbb{R}^d$.

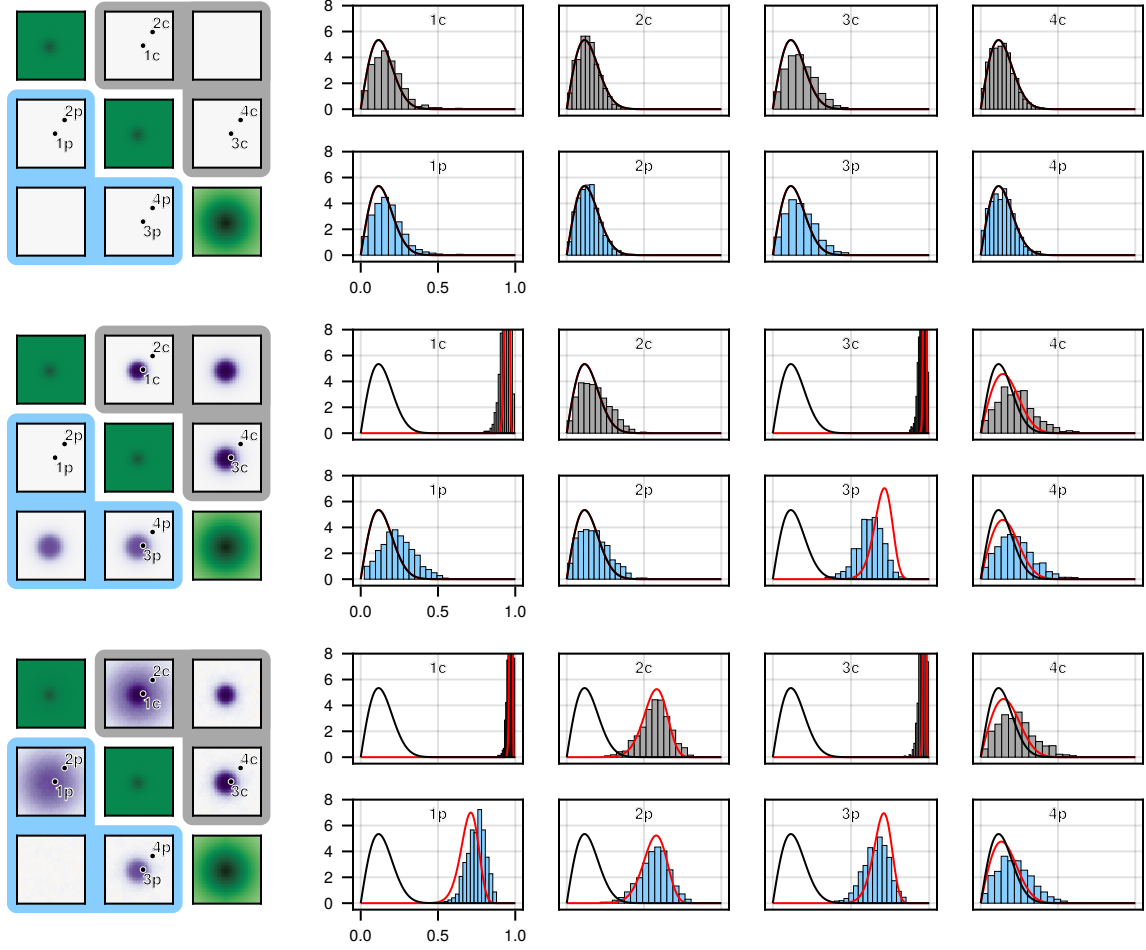


Figure 5: Results of the simulation study. The left column shows the true spectral matrix for each model, with the magnitude (partial) coherence in the upper (lower) triangle where both k_1 and k_2 range from -0.05 to 0.05 . The right hand column shows the estimated magnitude (partial) coherence on top (bottom), and asymptotic distribution (red line) and null distribution (black line). The rows correspond to models one to three from top to bottom.

SUPPLEMENTARY MATERIAL FOR SPECTRAL ESTIMATION FOR POINT PROCESSES AND RANDOM FIELDS

S1 Proofs of main results

S1.1 Proposition 1

Proof of Proposition 1. First recall the inverse relations

$$h_m(u) = \int_{\mathbb{R}^d} H_m(k) e^{2\pi i u \cdot k} dk, \quad h_m(z) = \int_{K_\Delta} H_m^{(\mathcal{G})}(k) e^{2\pi i z \cdot k} dk,$$

for $u \in \mathbb{R}^d$ and $z \in \mathcal{G}$ respectively. Then the argument is analogous to that given in Percival and Walden (1993) for time series aliasing. In particular, the collection of shifted sets, $\{k + z \odot \Delta \mid k \in K_\Delta\}$ for $z \in \mathbb{Z}^d$, form a partition of \mathbb{R}^d . Thus for $u \in \mathcal{G}$

$$\begin{aligned} \int_{K_\Delta} H_m^{(\mathcal{G})}(k) e^{2\pi i u \cdot k} dk &= h_m(u) \\ &= \int_{\mathbb{R}^d} H_m(k) e^{2\pi i u \cdot k} dk \\ &= \sum_{z \in \mathbb{Z}^d} \int_{K_\Delta} H_m(k + z \odot \Delta) e^{2\pi i u \cdot (k + z \odot \Delta)} dk \\ &= \int_{K_\Delta} \sum_{z \in \mathbb{Z}^d} H_m(k + z \odot \Delta) e^{2\pi i (u-v) \cdot (z \odot \Delta)} e^{2\pi i v \cdot (z \odot \Delta)} e^{2\pi i u \cdot k} dk \\ &= \int_{K_\Delta} \sum_{z \in \mathbb{Z}^d} H_m(k + z \odot \Delta) e^{2\pi i v \cdot (z \odot \Delta)} e^{2\pi i u \cdot k} dk \end{aligned}$$

because $u \in \mathcal{G} \Rightarrow (u - v) \cdot (z \odot \Delta) \in \mathbb{Z}$ and where the interchange of limits is valid because $\|H_m\|_1 < \infty$ (which will hold in our asymptotic framework by Assumption 2). Therefore

$$H_m^{(\mathcal{G})}(k) = \sum_{z \in \mathbb{Z}^d} H_m(k + z \odot \Delta) e^{2\pi i v \cdot (z \odot \Delta)},$$

for almost all $k \in K_\Delta$. Furthermore, because the tapers are bounded with bounded support, $\|h_m\|_1 < \infty$ and so H_m is uniformly continuous. Thus the result holds for all $k \in K_\Delta$. Finally, $H_m^{(\mathcal{G})}$ is periodic, so that if $\psi \in \{z \odot \Delta \mid z \in \mathbb{Z}\}$ then $H_m^{(\mathcal{G})}(k) = H_m^{(\mathcal{G})}(k + \psi)$ for all $k \in K_\Delta$. Thus the result holds for all $k \in \mathbb{R}^d$. \square

S1.2 Proposition 2

Proof of Proposition 2. Follows directly from Lemma S2, by setting $k_1 = k_2 = k$ and $m' = m$. \square

S1.3 Theorem 1

Proof of Theorem 1. Follows directly from Proposition S1, again setting $k_1 = k_2 = k$ and $m' = m$. \square

S1.4 Theorem 2

Proof. Asymptotic normality can be proved by establishing the convergence of all of the cumulants of the variables in question, provided they exist (Brillinger, 1982). From Proposition S2, all cumulants of order $r \geq 3$ converge to zero. In addition, we have

$$\mathbb{E}[J_{p;m,n}(k)] = 0, \quad \forall k \in \mathbb{R}^d.$$

Thus all that remains is to explore the remaining two cumulants (of a complex variable), namely the covariance and psuedo-covariance.⁵ The convergence of the covariance follows from Theorem 1, because

$$\begin{aligned}\text{cov}(J_{p;m,n}(k), J_{q;m,n}(k)) &= \mathbb{E} [J_{p;m,n}(k) \overline{J_{q;m,n}(k)}] \\ &= \mathbb{E} [I_{p,q;m,n}(k)] \\ &\rightarrow \tilde{f}_{p,q}(k).\end{aligned}$$

Finally the pseudo-covariance is given by

$$\begin{aligned}\mathcal{C}[J_{p;m,n}(k), J_{q;m,n}(k)] &= \text{cov}(J_{p;m,n}(k), \overline{J_{q;m,n}(k)}) \\ &= \text{cov}(J_{p;m,n}(k), J_{q;m,n}(-k)) \\ &\rightarrow \begin{cases} w_q(2k) \tilde{f}_{p,q}(k) & \text{if } 2k \in \Psi_p, \\ w_p(2k) \tilde{f}_{p,q}(-k) & \text{if } 2k \in \Psi_q \setminus \Psi_p, \\ 0 & \text{otherwise.} \end{cases}\end{aligned}$$

In the case when $m \neq m'$, the covariance and pseudo-covariance both converge to zero. Thus we have convergence in distribution as required.

For differing k , we may again apply Proposition S1 to show that the covariance and pseudo-covariance converge to zero under the assumptions of the Theorem. \square

S1.5 Theorem A1

Proof of Theorem A1. We have that

$$\text{var}(\hat{f}_{p,q;n}(k)) = \frac{1}{M_n^2} \sum_{m=1}^{M_n} \sum_{m'=1}^{M_n} \text{cov}(I_{p,q;m,n}(k), I_{p,q;m',n}(k)).$$

Now we have

$$\begin{aligned}&\text{cov}(I_{p,q;m,n}(k), I_{p,q;m',n}(k)) \\ &= \mathbb{E}[I_{p,q;m,n}(k) I_{p,q;m',n}(-k)] - \mathbb{E}[I_{p,q;m,n}(k)] \mathbb{E}[I_{p,q;m',n}(-k)] \\ &= \mathbb{E}[J_{p;m,n}(k) J_{q;m,n}(-k) J_{p;m',n}(-k) J_{q;m',n}(k)] - \mathbb{E}[I_{p,q;m,n}(k)] \mathbb{E}[I_{p,q;m',n}(k)] \\ &= \mathcal{C}[J_{p;m,n}(k), J_{q;m,n}(-k), J_{p;m',n}(-k), J_{q;m',n}(k)] \\ &\quad + \mathbb{E}[J_{p;m,n}(k) J_{p;m',n}(-k)] \mathbb{E}[J_{q;m,n}(-k) J_{q;m',n}(k)] \\ &\quad + \mathbb{E}[J_{p;m,n}(k) J_{q;m',n}(k)] \mathbb{E}[J_{q;m,n}(-k) J_{p;m',n}(-k)].\end{aligned}$$

Now the first of these terms converges to zero by Proposition S2. If $m \neq m'$, then the second and third terms also converge to zero. The diagonal terms converge to zero or $\tilde{f}_{p,q}(k)^2$ by Theorem 1. Thus the result follows. \square

S2 Lemmas for main theorems

S2.1 Covariance of spatial processes

The following Lemma enables us to work with weighted integrals and sums of the spatial processes.

Lemma S1. *Given Assumptions 1 hold. Without loss of generality, let ξ_1, ξ_2 be either marked point processes or integrated random fields, and ξ_3, ξ_4 be integrated random fields. Let $\phi_1, \phi_2, \phi_3, \phi_4$ be integrable functions with bounded support and integrable Fourier transforms, and let $\mathcal{G}_3, \mathcal{G}_4$ be a regular grids with sampling intervals Δ_3, Δ_4 and offset*

⁵Note that, as in the second-order case, there are more than one higher-order cumulants of interest for each combination of processes, namely all combinations of conjugates of the involved random variables; however, those cases are also covered by simply taking the negative of the wavenumber and using the same results.

v_3, v_4 . Then

$$\begin{aligned} \text{cov} \left(\int_{\mathbb{R}^d} \phi_1(s) \xi_1(ds), \int_{\mathbb{R}^d} \phi_2(s) \xi_2(ds) \right) &= \int_{\mathbb{R}^d} \Phi_1(-k) \overline{\Phi_2(-k)} f_{1,2}(k) dk, \\ \text{cov} \left(\int_{\mathbb{R}^d} \phi_1(s) \xi_1(ds), \int_{\mathbb{R}^d} \phi_3^{(\mathcal{G}_3)}(s) \xi_3(ds) \right) &= \int_{\mathbb{R}^d} \Phi_1(-k) \overline{\Phi_3^{(\mathcal{G}_3)}(-k)} f_{1,3}(k) dk, \\ \text{cov} \left(\int_{\mathbb{R}^d} \phi_3^{(\mathcal{G}_3)}(s) \xi_3(ds), \int_{\mathbb{R}^d} \phi_4^{(\mathcal{G}_4)}(s) \xi_4(ds) \right) &= \int_{\mathbb{R}^d} \Phi_3^{(\mathcal{G}_3)}(-k) \overline{\Phi_4^{(\mathcal{G}_4)}(-k)} f_{1,4}(k) dk. \end{aligned}$$

where Φ_j is the Fourier transform of ϕ_j , i.e. $\Phi_j(k) = \int_{\mathbb{R}^d} \phi_j(u) e^{-2\pi i u \cdot k} du$, $k \in \mathbb{R}^d$.

Therefore if ξ_p, ξ_q are either marked point processes or integrated random fields and ϕ_p, ϕ_q are integrable functions with bounded support and integrable Fourier transforms, or sampled versions of such functions if the corresponding process is an integrated random field, then from the previous cases

$$\text{cov} \left(\int_{\mathbb{R}^d} \phi_p(s) \xi_p(ds), \int_{\mathbb{R}^d} \phi_q(s) \xi_q(ds) \right) = \int_{\mathbb{R}^d} \Phi_p(-k) \overline{\Phi_q(-k)} f_{p,q}(k) dk.$$

Proof. We have that for $j \in \{1, \dots, 4\}$, $\phi_j(u) = \int_{\mathbb{R}^d} \Phi_j(k) e^{2\pi i k \cdot s} dk$. Begin with the first case,

$$\begin{aligned} LHS &= \text{cov} \left(\int_{\mathbb{R}^d} \phi_1(s) \xi_1(ds), \int_{\mathbb{R}^d} \phi_2(s) \xi_2(ds) \right) \\ &= \int_{\mathbb{R}^d} \int_{\mathbb{R}^d} \phi_1(s_1) \overline{\phi_2(s_2)} \check{c}_{1,2}(s_1 - s_2) \\ &= \int_{\mathbb{R}^d} \int_{\mathbb{R}^d} \int_{\mathbb{R}^d} \Phi_1(-k) e^{-2\pi i k \cdot s_1} dk \overline{\phi_2(s_2)} \check{c}_{1,2}(s_1 - s_2) ds_1 ds_2 \\ &= \int_{\mathbb{R}^d} \Phi_1(-k) \int_{\mathbb{R}^d} \overline{\phi_2(s_2)} e^{-2\pi i k \cdot s_2} \int_{\mathbb{R}^d} \check{c}_{1,2}(s_1 - s_2) ds_1 e^{-2\pi i k \cdot u} du dk \\ &= \int_{\mathbb{R}^d} \Phi_1(-k) \overline{\Phi_2(-k)} f_{1,2}(k) dk \end{aligned}$$

where the interchange of limits is justified because ϕ_1, ϕ_2 are assumed to be integrable; and $\check{C}_{p,q}$ separates into finitely many atoms and an absolutely continuous part from Assumption 1, making $\check{c}_{p,q}$ integrable (Daley and Vere-Jones, 2003).

Now in the second case, write Y_3 for the random field

$$\begin{aligned} \text{cov} \left(\int_{\mathbb{R}^d} \phi_1(u) \xi_1(du), Y_3(s) \right) &= \int_{\mathbb{R}^d} \phi_1(u) \check{c}_{1,3}(u - s) du \\ &= \int_{\mathbb{R}^d} \int_{\mathbb{R}^d} \Phi_1(-k) e^{-2\pi i k \cdot u} dk \check{c}_{1,3}(u - s) du \\ &= \int_{\mathbb{R}^d} \Phi_1(-k) \int_{\mathbb{R}^d} \check{c}_{1,3}(u - s) e^{-2\pi i k \cdot u - s} du e^{-2\pi i k \cdot s} dk \\ &= \int_{\mathbb{R}^d} \Phi_1(-k) f_{1,3}(k) e^{-2\pi i s \cdot k} dk, \end{aligned}$$

where the interchange is justified as both Φ_1 and $\check{c}_{1,3}$ are integrable. Therefore

$$\begin{aligned} LHS &= \text{cov} \left(\int_{\mathbb{R}^d} \phi_1(u) \xi_1(du), \int_{\mathbb{R}^d} \phi_3^{(\mathcal{G}_3)}(u) \xi_3(du) \right) \\ &= \prod_{j=1}^d \Delta_{3;j} \sum_{s \in \mathcal{G}} \overline{\phi_3^{(\mathcal{G}_3)}(u)} \int_{\mathbb{R}^d} \Phi_1(-k) f_{1,3}(k) e^{-2\pi i s \cdot k} dk \\ &= \int_{\mathbb{R}^d} \Phi_1(-k) f_{1,3}(k) \prod_{j=1}^d \Delta_{3;j} \sum_{s \in \mathcal{G}} \overline{\phi_3^{(\mathcal{G}_3)}(u)} e^{-2\pi i s \cdot k} dk \\ &= \int_{\mathbb{R}^d} \Phi_1(-k) \overline{\Phi_3^{(\mathcal{G})}(-k)} f_{p,q}(k) dk, \end{aligned}$$

where the interchange is justified because the summands are only non-zero for a finite subset of \mathcal{G}_3 (as ϕ_3 has bounded support).

For the final case, $\check{c}_{3,4}$ is continuous by assumption, so we have the inverse relation

$$\check{c}_{3,4}(u) = \int_{\mathbb{R}^d} f_{3,4}(k) e^{2\pi i u \cdot k} dk.$$

Therefore, writing $\Delta_{3;j}$ for the j^{th} element of Δ_3

$$\begin{aligned} LHS &= \text{cov} \left(\int_{\mathbb{R}^d} \phi_3^{(\mathcal{G}_3)}(u) \xi_3(du), \int_{\mathbb{R}^d} \phi_4^{(\mathcal{G}_4)}(u) \xi_4(du) \right) \\ &= \prod_{j=1}^d \Delta_{3;j} \Delta_{4;j} \sum_{u \in \mathcal{G}_3} \sum_{s \in \mathcal{G}_4} \phi_3(u) \overline{\phi_4(s)} \check{c}_{3,4}(u-s) \\ &= \prod_{j=1}^d \Delta_{3;j} \Delta_{4;j} \sum_{u \in \mathcal{G}_3} \sum_{s \in \mathcal{G}_4} \phi_3(u) \overline{\phi_4(s)} \int_{\mathbb{R}^d} f_{3,4}(k) e^{2\pi i(u-s) \cdot k} dk \\ &= \int_{\mathbb{R}^d} \Phi_3^{(\mathcal{G}_3)}(-k) \overline{\Phi_4^{(\mathcal{G}_4)}(-k)} f_{3,4}(k) dk, \end{aligned}$$

where the final equality holds because they are both finite sums. The general statement is covered by these three cases. \square

Lemma S2. *Given the processes satisfy Assumption 1 and the tapers satisfy Assumption 2,*

$$\mathbb{E} \left[J_{p;m,n}(k_1) \overline{J_{q;m',n}(k_2)} \right] = \int_{\mathbb{R}^d} H_{p;m,n}(k_1 - k') \overline{H_{q;m',n}(k_2 - k')} f_{p,q}(k') dk' \quad (1)$$

for any $k_1, k_2 \in \mathbb{R}^d$.

Proof. The assumption that λ_p, λ_q are known implies that the expectation of the tapered Fourier transform is zero, and so

$$\mathbb{E} \left[J_{p;m,n}(k_1) \overline{J_{q;m',n}(k_2)} \right] = \text{cov} (J_{p;m,n}(k_1), J_{q;m,n}(k_2)).$$

Assumption 2 implies that we may use Lemma S1, setting $\phi_p(s) = h_{p;m}(s) e^{-2\pi i s \cdot k_1}$ and $\phi_q(s) = h_{q;m'}(s) e^{-2\pi i s \cdot k_2}$. Note

$$\begin{aligned} \Phi_p(k) &= \int_{\mathbb{R}^d} h_{p;m}(s) e^{-2\pi i s \cdot k_1} e^{-2\pi i s \cdot k} ds \\ &= H_{p;m}(k_1 + k). \end{aligned}$$

The result then follows from Lemma S1. \square

S2.2 Properties of the sampled taper

Lemma S3. *The following properties hold*

$$\begin{aligned} \forall k \in \mathbb{R}^d, \quad w_p(k) &= \overline{w_p(-k)}, \\ \forall k, k' \in \mathbb{R}^d, \quad w_p(k + k') &= w_p(k) w_p(k'), \\ \psi_1, \psi_2 \in \Psi_p &\Rightarrow \psi_1 \pm \psi_2 \in \Psi_p. \end{aligned}$$

Proof. This is immediate from the Definition. \square

Now we have some useful intermediary auxillary results.

Lemma S4. *Given Assumptions 2 and 4, for any process, we have that for $\psi \in \Psi_p \cap \Psi_q$, the following cases hold. If $k_1 \in \Psi_p$ and $k_2 \in \Psi_q$, then*

$$\int_{B_{b_n}(\psi)} H_{p;m,n}(k_1 - k) \overline{H_{q;m,n}(k_2 - k)} dk \rightarrow w_p(\psi - k_1) \overline{w_q(\psi - k_2)},$$

if $m \neq m'$ or $k_1 \notin \Psi_p$ or $k_2 \notin \Psi_q$ then

$$\int_{B_{b_n}(\psi)} H_{p;m,n}(k_1 - k) \overline{H_{q;m',n}(k_2 - k)} dk \rightarrow 0.$$

Proof. Let $\psi \in \Psi_p \cap \Psi_q$, then applying Proposition 1

$$\int_{B_{b_n}(\psi)} H_{p;m,n}(k_1 - k) \overline{H_{q;m',n}(k_2 - k)} dk = \sum_{\psi_1 \in \Psi_p} \sum_{\psi_2 \in \Psi_q} w_p(\psi_1) \overline{w_q(\psi_2)} T(\psi_1, \psi_2) \quad (2)$$

where (suppressing the dependence of $T(\psi_1, \psi_2)$ on k_1, k_2 in our notation)

$$T(\psi_1, \psi_2) = \int_{B_{b_n}(\psi)} H_{m,n}(k_1 - k + \psi_1) \overline{H_{m',n}(k_2 - k + \psi_2)} dk.$$

Now we can bound the summands as follows

$$\begin{aligned} |T(\psi_1, \psi_2)|^2 &= \left| \int_{B_{b_n}(\psi)} H_{m,n}(k_1 - k + \psi_1) \overline{H_{m',n}(k_2 - k + \psi_2)} dk \right|^2 \\ &\leq \int_{B_{b_n}(\psi)} |H_{m,n}(k_1 - k + \psi_1)|^2 dk \int_{B_{b_n}(\psi)} |H_{m',n}(k_2 - k + \psi_2)|^2 dk \\ &= \int_{B_{b_n}(k_1 + \psi_1 - \psi)} |H_{m,n}(k)|^2 dk \int_{B_{b_n}(k_2 + \psi_2 - \psi)} |H_{m',n}(k)|^2 dk. \end{aligned}$$

Now if $\psi_1 + k_1 \neq \psi$, there is some N such that for any $n > N$, $|\psi_1 + k_1 - \psi| > 2b_n$. Therefore for such $n > N$ we have that $B_{b_n}(k_1 + \psi_1 - \psi) \cap B_{b_n}(0) = \emptyset$, so $B_{b_n}(k_1 + \psi_1 - \psi) \subseteq \mathbb{R}^d \setminus B_{b_n}(0)$ and therefore

$$\int_{B_{b_n}(k_1 + \psi_1 - \psi)} |H_{m,n}(k)|^2 dk \leq \int_{\mathbb{R}^d \setminus B_{b_n}(0)} |H_{m,n}(k)|^2 dk.$$

By assumption, this converges to zero, and so

$$|T(\psi_1, \psi_2)|^2 \rightarrow 0$$

as $n \rightarrow \infty$. An equivalent argument holds for $\psi_2 + k_2 \neq \psi$.

If $\psi_1 + k_1 = \psi_2 + k_2 = \psi$ then

$$\begin{aligned} T(\psi_1, \psi_2) &= \int_{B_{b_n}(\psi)} H_{m,n}(k_1 - k + \psi_1) \overline{H_{m',n}(k_2 - k + \psi_2)} dk \\ &= \int_{B_{b_n}(0)} H_{m,n}(k) \overline{H_{m',n}(k)} dk. \end{aligned}$$

If $m = m'$, then $T(\psi_1, \psi_2) \rightarrow 1$ as $n \rightarrow \infty$. Otherwise, we see that

$$\begin{aligned} T(\psi_1, \psi_2) &= \int_{B_{b_n}(0)} H_{m,n}(k) \overline{H_{m',n}(k)} dk \\ &= \int_{\mathbb{R}^d} H_{m,n}(k) \overline{H_{m',n}(k)} dk - \int_{\mathbb{R}^d \setminus B_{b_n}(0)} H_{m,n}(k) \overline{H_{m',n}(k)} dk \\ &= 0 - \int_{\mathbb{R}^d \setminus B_{b_n}(0)} H_{m,n}(k) \overline{H_{m',n}(k)} dk, \end{aligned}$$

and so by Cauchy-Schwarz,

$$|T(\psi_1, \psi_2)|^2 \leq \int_{\mathbb{R}^d \setminus B_{b_n}(0)} |H_{m,n}(k)|^2 dk \int_{\mathbb{R}^d \setminus B_{b_n}(0)} |H_{m',n}(k)|^2 dk \rightarrow 0$$

as $n \rightarrow \infty$.

Within the sum in (2), if $k_1 \in \Psi_p$ and $k_2 \in \Psi_q$, then $\psi - k_1 \in \Psi_p$ and $\psi - k_2 \in \Psi_q$, and so those terms survive provided $m = m'$, meaning in this case

$$\int_{B_{b_n}(\psi)} H_{p;m,n}(k_1 - k) \overline{H_{q;m,n}(k_2 - k)} dk \rightarrow w_p(\psi - k_1) \overline{w_q(\psi - k_2)},$$

as $n \rightarrow \infty$. Otherwise, say $k_1 \notin \Psi_p$, then $\psi - k_1 \notin \Psi_p$ and so no term survives, similarly for k_2 , and of course for $m \neq m'$. Therefore

$$\int_{B_{b_n}(\psi)} H_{p;m,n}(k_1 - k) \overline{H_{q;m',n}(k_2 - k)} dk \rightarrow 0,$$

as $n \rightarrow \infty$ as required. \square

Lemma S5. Assume that Assumption 1 and Assumption 4 hold. For $k_1, k_2 \in \mathbb{R}^d$, let

$$T_n(k) = \int_{B_{b_n}(k)} H_{p;m,n}(k_1 - k') \overline{H_{q;m',n}(k_2 - k')} f_{p,q}(k') dk'$$

a function of the location of the ball over which the integral is evaluated (whose dependence on k_1, k_2 is suppressed in our notation). Then for all $\psi \in \Psi_p \cap \Psi_q$,

$$\begin{aligned} T_n(k_1 + \psi) &\rightarrow \begin{cases} w_p(\psi) \overline{w_q(\psi + [k_1 - k_2])} f_{p,q}(\psi + k_1) & \text{if } k_2 - k_1 \in \Psi_q \text{ and } m = m' \\ 0 & \text{otherwise,} \end{cases} \\ T_n(k_2 + \psi) &\rightarrow \begin{cases} w_p(\psi + [k_2 - k_1]) \overline{w_q(\psi)} f_{p,q}(\psi + k_2) & \text{if } k_1 - k_2 \in \Psi_p \text{ and } m = m', \\ 0 & \text{otherwise.} \end{cases} \end{aligned}$$

Proof. Consider the first case

$$\begin{aligned} T_n(k_1 + \psi) &= \int_{B_{b_n}(k_1 + \psi)} H_{p;m,n}(k_1 - k') \overline{H_{q;m',n}(k_2 - k')} dk' f_{p,q}(k_1 + \psi) \\ &\quad + \int_{B_{b_n}(k_1 + \psi)} H_{p;m,n}(k_1 - k') \overline{H_{q;m',n}(k_2 - k')} [f_{p,q}(k') - f_{p,q}(k_1 + \psi)] dk'. \end{aligned}$$

For the first term

$$\begin{aligned} &\int_{B_{b_n}(k_1 + \psi)} H_{p;m,n}(k_1 - k') \overline{H_{q;m',n}(k_2 - k')} dk' \\ &= \int_{B_{b_n}(\psi)} H_{p;m,n}(-k'') \overline{H_{q;m',n}([k_2 - k_1] - k')} dk' \\ &\rightarrow \begin{cases} w_p(\psi) \overline{w_q(\psi - [k_2 - k_1])} & \text{if } m = m' \text{ and } k_2 - k_1 \in \Psi_q, \\ 0 & \text{otherwise,} \end{cases} \end{aligned}$$

from Lemma S4, because $0 \in \Psi_p$.

Now the second part satisfies

$$\begin{aligned} &\left| \int_{B_{b_n}(k_1 + \psi)} H_{p;m,n}(k_1 - k') \overline{H_{q;m',n}(k_2 - k')} [f_{p,q}(k') - f_{p,q}(k_1 + \psi)] dk' \right| \\ &\leq \int_{B_{b_n}(\psi)} \left| H_{p;m,n}(-k') \overline{H_{q;m',n}(k_2 - k_1 - k')} \right| dk' \sup_{k'' \in B_{b_n}(k_1 + \psi)} |f_{p,q}(k'') - f_{p,q}(k_1 + \psi)| \\ &\rightarrow 0 \end{aligned}$$

because $f_{p,q}$ is continuous and by Cauchy-Schwarz

$$\begin{aligned} &\left| \int_{B_{b_n}(\psi)} \left| H_{p;m,n}(-k') \overline{H_{q;m',n}(k_2 - k_1 - k')} \right| dk' \right|^2 \\ &\leq \int_{B_{b_n}(\psi)} |H_{p;m,n}(-k')|^2 dk' \int_{B_{b_n}(\psi)} |H_{q;m',n}(k_2 - k_1 - k')|^2 dk' \end{aligned}$$

whose limit is finite by Lemma S4. The proof for the other case is analogous, and thus omitted. \square

Proposition S1. Let $k_1, k_2 \in \mathbb{R}^d$, $n \in \mathbb{N}$, $m, m' \in \{1, \dots, M\}$ and $p, q \in \{1, \dots, P\}$. Assume that Assumptions 1 and Assumptions 2, 4 hold. Write

$$L = \int_{\mathbb{R}^d} H_{p;m,n}(k_1 - k') \overline{H_{q;m',n}(k_2 - k')} f_{p,q}(k') dk$$

Then if $m \neq m'$ or $k_2 - k_1 \notin \Psi_p \cup \Psi_q$, $L \rightarrow 0$ as $n \rightarrow \infty$. Otherwise

$$L \rightarrow \begin{cases} w_q(k_2 - k_1) \tilde{f}_{p,q}(k_1) & \text{if } k_2 - k_1 \in \Psi_q \\ w_p(k_2 - k_1) \tilde{f}_{p,q}(k_2) & \text{if } k_2 - k_1 \in \Psi_p \setminus \Psi_q. \end{cases}$$

Proof. Letting $B_{p,q;b_n} = \bigcup_{\psi_1, \psi_2 \in \Psi_p \cap \Psi_q} B_{b_n}(\psi_1 + k_1) \cup B_{b_n}(\psi_2 + k_2)$ then partition the space as

$$\begin{aligned} L &= \sum_{\psi \in \Psi_p \cap \Psi_q} \int_{B_{b_n}(k_1 + \psi)} H_{p;m,n}(k_1 - k') \overline{H_{q;m',n}(k_2 - k')} f_{p,q}(k') dk' \\ &\quad + \sum_{\psi \in \Psi_p \cap \Psi_q} \int_{B_{b_n}(k_2 + \psi)} H_{p;m,n}(k_1 - k') \overline{H_{q;m',n}(k_2 - k')} f_{p,q}(k') dk' \\ &\quad - \sum_{\psi_1 \in \Psi_p \cap \Psi_q} \sum_{\psi_2 \in \Psi_p \cap \Psi_q} \int_{B_{b_n}(k_1 + \psi_1) \cap B_{b_n}(k_2 + \psi_2)} H_{p;m,n}(k_1 - k') \overline{H_{q;m',n}(k_2 - k')} f_{p,q}(k') dk' \\ &\quad + \int_{\mathbb{R}^d \setminus B_{p,q;b_n}} H_{p;m,n}(k_1 - k') \overline{H_{q;m',n}(k_2 - k')} f_{p,q}(k') dk'. \end{aligned}$$

The first two terms are easily dealt with from Lemma S5. Now for the third term, if $k_1 + \psi_1 \neq k_2 + \psi_2$

$$B_{b_n}(k_1 + \psi_1) \cap B_{b_n}(k_2 + \psi_2) \rightarrow \emptyset,$$

making the summands $o(1)$ in this case. Thus

$$\begin{aligned} &\sum_{\psi_1 \in \Psi_p \cap \Psi_q} \sum_{\psi_2 \in \Psi_p \cap \Psi_q} \int_{B_{b_n}(k_1 + \psi_1) \cap B_{b_n}(k_2 + \psi_2)} H_{p;m,n}(k_1 - k') \overline{H_{q;m',n}(k_2 - k')} f_{p,q}(k') dk' \\ &= \sum_{\psi_1 \in \Psi_p \cap \Psi_q} \sum_{\psi_2 \in \Psi_p \cap \Psi_q} \mathbb{1}_{\psi_1 = k_2 - k_1 + \psi_2} \int_{B_{b_n}(k_2 + \psi_2)} H_{p;m,n}(k_1 - k') \overline{H_{q;m',n}(k_2 - k')} f_{p,q}(k') dk' + o(1) \\ &= \mathbb{1}_{\Psi_p \cap \Psi_q}(k_1 - k_2) \sum_{\psi_2 \in \Psi_p \cap \Psi_q} \int_{B_{b_n}(k_2 + \psi_2)} H_{p;m,n}(k_1 - k') \overline{H_{q;m',n}(k_2 - k')} f_{p,q}(k') dk' + o(1) \\ &= \mathbb{1}_{\Psi_p \cap \Psi_q}(k_1 - k_2) \sum_{\psi \in \Psi_p \cap \Psi_q} w_p(\psi - k_1 + k_2) \overline{w_q(\psi)} f_{p,q}(\psi + k_2) + o(1). \end{aligned}$$

Now for the final term we have

$$\int_{\mathbb{R}^d \setminus B_{p,q;b_n}} H_{p;m,n}(k_1 - k) \overline{H_{q;m',n}(k_2 - k)} f_{p,q}(k) dk = \sum_{\psi_1 \in \Psi_p} \sum_{\psi_2 \in \Psi_q} w_p(\psi_1) \overline{w_q(\psi_2)} S(\psi_1, \psi_2),$$

where, again suppressing dependence on the fixed k_1, k_2 , we define

$$S(\psi_1, \psi_2) = \int_{\mathbb{R}^d \setminus B_{p,q;b_n}} H_{m,n}(k_1 - k + \psi_1) \overline{H_{m',n}(k_2 - k + \psi_2)} f_{p,q}(k) dk.$$

Now we have

$$\begin{aligned} |S(\psi_1, \psi_2)|^2 &\leq \|f_{p,q}(k)\|_\infty^2 \int_{\mathbb{R}^d \setminus B_{p,q;b_n}} |H_{m,n}(k_1 + \psi_1 - k)|^2 dk \int_{\mathbb{R}^d \setminus B_{p,q;b_n}} |H_{m',n}(k_2 + \psi_2 - k)|^2 dk \\ &\leq \|f_{p,q}(k)\|_\infty^2 \int_{\mathbb{R}^d \setminus B_{b_n}(\psi_1 + k_1)} |H_{m,n}(k_1 + \psi_1 - k)|^2 dk \|H_{m',n}\|_2^2 \\ &\rightarrow 0 \end{aligned}$$

because $B_{b_n}(\psi_1 + k_1) \subset B_{p,q;b_n}$ and the cross-spectra is bounded. Therefore as $n \rightarrow \infty$

$$\begin{aligned}
& \int_{\mathbb{R}^d} H_{p;m,n}(k_1 - k') \overline{H_{q;m',n}(k_2 - k')} f_{p,q}(k') dk' \\
& \rightarrow \delta_{m,m'} \left\{ \mathbb{1}_{\Psi_q}(k_1 - k_2) \sum_{\psi \in \Psi_p \cap \Psi_q} w_p(\psi) \overline{w_q(\psi - k_2 + k_1)} f_{p,q}(\psi + k_1) \right. \\
& \quad + \mathbb{1}_{\Psi_p}(k_1 - k_2) \sum_{\psi \in \Psi_p \cap \Psi_q} w_p(\psi - k_1 + k_2) \overline{w_q(\psi)} f_{p,q}(\psi + k_2) \\
& \quad \left. - \mathbb{1}_{\Psi_p \cap \Psi_q}(k_1 - k_2) \sum_{\psi \in \Psi_p \cap \Psi_q} w_p(\psi - k_1 + k_2) \overline{w_q(\psi)} f_{p,q}(\psi + k_2) \right\} \\
& = \delta_{m,m'} \left\{ \mathbb{1}_{\Psi_q}(k_1 - k_2) \sum_{\psi \in \Psi_p \cap \Psi_q} w_p(\psi) \overline{w_q(\psi - k_2 + k_1)} f_{p,q}(\psi + k_1) \right. \\
& \quad \left. + \mathbb{1}_{\Psi_p \setminus \Psi_q}(k_1 - k_2) \sum_{\psi \in \Psi_p \cap \Psi_q} w_p(\psi - k_1 + k_2) \overline{w_q(\psi)} f_{p,q}(\psi + k_2) \right\} \\
& = \delta_{m,m'} \left\{ \mathbb{1}_{\Psi_q}(k_1 - k_2) \overline{w_q(k_1 - k_2)} \sum_{\psi \in \Psi_p \cap \Psi_q} w_p(\psi) \overline{w_q(\psi)} f_{p,q}(\psi + k_1) \right. \\
& \quad \left. + \mathbb{1}_{\Psi_p \setminus \Psi_q}(k_1 - k_2) w_p(k_2 - k_1) \sum_{\psi \in \Psi_p \cap \Psi_q} w_p(\psi) \overline{w_q(\psi)} f_{p,q}(\psi + k_2) \right\} \\
& = \delta_{m,m'} \left\{ \mathbb{1}_{\Psi_q}(k_1 - k_2) w_q(k_2 - k_1) \tilde{f}_{p,q}(k_1) \right. \\
& \quad \left. + \mathbb{1}_{\Psi_p \setminus \Psi_q}(k_1 - k_2) w_p(k_2 - k_1) \tilde{f}_{p,q}(k_2) \right\}.
\end{aligned}$$

as $n \rightarrow \infty$, where we used the properties of w_p, w_q, Ψ_p and Ψ_q given in Lemma S3. \square

S2.3 Higher-order properties

We now require a few useful results, which are a variation of the results in Appendix 2 of Brillinger (1982), though we require that the tapers can be different, and need to deal with aliasing. We will require Hölder's inequality, which says for f, g measurable,

$$\|fg\|_1 \leq \|f\|_p \|g\|_q \quad \text{if } 1/p + 1/q = 1,$$

and Young's inequality (Young, 1912) i.e. for $f \in L_p(\mathbb{R}^d), g \in L_q(\mathbb{R}^d)$

$$\|f * g\|_r \leq \|f\|_p \|g\|_q \quad \text{if } 1/p + 1/q = 1 + 1/r.$$

Lemma S6. For $r \geq 3$, consider some functions $A_{j,n} : \mathbb{R}^d \rightarrow \mathbb{C}$ for $1 \leq j \leq r$ and $n \in \mathbb{N}$ such that $\|A_{j,n}\|_1 < \infty$ and $\|A_{j,n}\|_2 < \infty$ and let

$$\tilde{I}_{A,n}(x) = \int_{\mathbb{R}^d} \cdots \int_{\mathbb{R}^d} \left| \prod_{j=1}^{r-1} A_{j,n}(k_j) \right\} A_{r,n} \left(x - \sum_{j=1}^{r-1} k_j \right) dk_1 \cdots dk_{r-1}, \quad x \in \mathbb{R}^d.$$

Then

$$\tilde{I}_{A,n}(x) \leq \prod_{j=1}^r \left(\int_{\mathbb{R}^d} |A_{j,n}(k)|^{\frac{r}{r-1}} dk \right)^{\frac{r-1}{r}}.$$

Proof. Firstly we have

$$\begin{aligned}
\int_{\mathbb{R}^d} |A_{j,n}(k)|^{\frac{r}{r-1}} dk &= \left\| A_{j,n}^{\frac{2}{r-1}} \right\|_1 \left\| A_{j,n}^{\frac{r-2}{r-1}} \right\|_1 \\
&\leq \left\| A_{j,n}^{\frac{2}{r-1}} \right\|_{r-1} \left\| A_{j,n}^{\frac{r-2}{r-1}} \right\|_{\frac{r-1}{r-2}} \\
&= \left(\int_{\mathbb{R}^d} |A_{j,n}(k)|^2 dk \right)^{\frac{1}{r-1}} \left(\int_{\mathbb{R}^d} |A_{j,n}(k)| dk \right)^{\frac{r-2}{r-1}} \\
&< \infty
\end{aligned}$$

from Hölder's inequality and by the assumption of finiteness of $\|A_{j,n}\|_1$ and $\|A_{j,n}\|_2$.

Following the approach of Brillinger (1982), begin by making the substitution

$$\begin{aligned}
k'_1 &= k_1 \\
k'_j &= k_j + k'_{j-1} \quad \text{for } 2 \leq j \leq r-1,
\end{aligned}$$

then we get

$$\begin{aligned}
\tilde{I}_{A,n}(x) &= \int_{\mathbb{R}^d} \cdots \int_{\mathbb{R}^d} |H_{m_1,n}(k'_1) \left\{ \prod_{j=2}^{r-1} A_{j,n}(k'_j - k'_{j-1}) \right\} A_{r,n}(x - k'_{r-1})| dk'_1 \cdots dk'_{r-1} \\
&= \int_{\mathbb{R}^d} |\phi_{r-1}(k) A_{r,n}(x - k)| dk \\
&= \left\| \phi_{r-1} A_{r,n}^{(x)} \right\|_1,
\end{aligned}$$

where

$$\begin{aligned}
A_{r,n}^{(x)}(k) &= A_{r,n}(x - k) \\
\phi_{1,n}(k) &= A_{1,n}(k), \\
\phi_{j,n}(k) &= \int_{\mathbb{R}^d} |A_{j,n}(k - k') \phi_{j-1}(k')| dk,
\end{aligned}$$

for $2 \leq j \leq r-1$.

Now we have by Hölder's inequality

$$\left\| \phi_{r-1} A_{r,n}^{(x)} \right\|_1 \leq \left\| A_{r,n}^{(x)} \right\|_{\frac{r}{r-1}} \left\| \phi_{r-1,n} \right\|_r = \|A_{r,n}\|_{\frac{r}{r-1}} \|\phi_{r-1,n}\|_r$$

and by definition and Young's inequality

$$\begin{aligned}
\|\phi_{1,n}\|_{\frac{r}{r-1}} &= \|A_{1,n}\|_{\frac{r}{r-1}} \\
\|\phi_{j,n}\|_{\frac{r}{r-j}} &= \|A_{j,n} * \phi_{j-1}\|_{\frac{r}{r-1}} \\
&\leq \|A_{j,n}\|_{\frac{r}{r-1}} \|\phi_{j-1,n}\|_{\frac{r}{r-(j-1)}}
\end{aligned}$$

for $2 \leq j \leq r-1$. Here Young's inequality applies because, $\|A_{j,n}\|_{\frac{r}{r-1}}$ is finite, and $\|\phi_{j-1,n}\|_{\frac{r}{r-(j-1)}}$ is therefore finite by induction. Applying this recursively we obtain

$$\tilde{I}_{A,n}(x) \leq \prod_{j=1}^r \|A_{j,n}\|_{\frac{r}{r-1}}$$

giving the result. \square

Definition S1. Let $\check{c}_{p_1, \dots, p_r}$ be the r^{th} reduced cumulant density of the processes $\xi_{p_1}, \dots, \xi_{p_r}$ (in the generalised function sense). Assume without loss of generality that the first t such processes are random fields sampled on \mathcal{G} , define the corresponding r^{th} -order aliased cumulant spectra as

$$\tilde{f}_{p_1, \dots, p_r}(k_1, \dots, k_{r-1}) = \sum_{u_1 \in \mathcal{G}} \cdots \sum_{u_t \in \mathcal{G}} \int_{\mathbb{R}^d} \cdots \int_{\mathbb{R}^d} e^{-2\pi i \sum_{j=1}^{r-1} k_j \cdot u_j} \check{c}_{p_1, \dots, p_r}(u_1, \dots, u_r) du_{t+1} \cdots du_r.$$

Lemma S7. Consider ϕ_1, \dots, ϕ_r which are functions or generalised functions as in Lemma S1, but such that for the random fields recorded on grids the grid is the same \mathcal{G} with Nyquist box K_Δ . Assume without loss of generality that the first t such processes are random fields sampled on \mathcal{G} , then

$$\begin{aligned} & \mathbb{C} \left[\int_{\mathbb{R}^d} \phi_1(s_1) ds_1, \dots, \int_{\mathbb{R}^d} \phi_r(s_r) ds_r \right] \\ &= \int_{\mathbb{R}^d} \dots \int_{\mathbb{R}^d} \tilde{f}_{p_1, \dots, p_r}(k_1, \dots, k_{r-1}) \prod_{j=1}^r \Phi_j(-k_j) dk_1 \dots dk_{r-1} \end{aligned}$$

where $k_r = -\sum_{j=1}^{r-1} k_j$ and $\mathbb{C}[X_1, \dots, X_r]$ denotes the joint cumulant of the random variables X_1, \dots, X_r (see e.g. Brillinger (1974) for a definition).

Proof. Say wlog that the first t are sampled on \mathcal{G} , then we have

$$\begin{aligned} & \mathbb{C} \left[\int_{\mathbb{R}^d} \phi_1(s_1) ds_1, \dots, \int_{\mathbb{R}^d} \phi_r(s_r) ds_r \right] \\ &= \sum_{s_1 \in \mathcal{G}} \dots \sum_{s_t \in \mathcal{G}} \int_{\mathbb{R}^d} \dots \int_{\mathbb{R}^d} \prod_{j=1}^r \phi_j(s_j) \check{c}_{p_1, \dots, p_r}(s_1 - s_r, \dots, s_{r-1} - s_r) ds_{t+1} \dots ds_r \\ &= \sum_{s_1 \in \mathcal{G}} \dots \sum_{s_t \in \mathcal{G}} \int_{\mathbb{R}^d} \dots \int_{\mathbb{R}^d} \prod_{j=1}^r \int_{\mathbb{R}^d} \Phi(-k_j) e^{-2\pi i k_j \cdot s_j} dk_j \check{c}_{p_1, \dots, p_r}(s_1 - s_r, \dots, s_{r-1} - s_r) ds_{t+1} \dots ds_r \\ &= \int_{\mathbb{R}^d} \dots \int_{\mathbb{R}^d} \prod_{j=1}^r \Phi_j(-k_j) \tilde{f}_{p_1, \dots, p_r}(k_1, \dots, k_{r-1}) \delta\left(\sum_{j=1}^r k_j\right) dk_1 \dots dk_r \end{aligned}$$

giving the required result. \square

For convenience, it is useful to embed the different grids into one grid which contains all of them. For any grid of interest (with offset and spacing to finite precision) this is always possible, and we can zero out the tapers outside of their respective grids so that the tapered Fourier transforms are not changed. Call this supergrid \mathcal{G} .

Proposition S2. For processes $\xi_{p_1}, \dots, \xi_{p_r}$ with $r \geq 3$ and $p_1, \dots, p_r \in \{1, \dots, P\}$, and $k_1, \dots, k_r \in \mathbb{R}^d$, provided the grids can all be embedded on some supergrid \mathcal{G} with offset v and spacing Δ , then we have

$$\mathbb{C}[J_{p_1; m_1, n}(k_1), \dots, J_{p_r; m_r, n}(k_r)] \rightarrow 0$$

as $n \rightarrow \infty$.

Proof. In order to deal with the different grids, we will create new taper functions which are defined on one grid, but zero out any terms which are not in the original grid, and match terms which are in the original grid. Let

$$\phi_j(s) = a_{j,n}(s) e^{-2\pi i k_j \cdot s},$$

where for $t < j < r$ (continuously recorded process) we let

$$a_{j,n}(s) = h_{m_j, n}(s),$$

and for $1 \leq j \leq t$ (processes recorded on a grid) we let

$$a_{j,n}(s) = \mathcal{I}[\tilde{a}_{j,n}](s)$$

where \mathcal{I} denotes linear interpolation of a sequence (see Section S4) and

$$\tilde{a}_{j,n}(s) = \prod_{l=1}^d \Delta_{p;l} h_{m_j, n}(s) e^{-2\pi i k_j \cdot s} \mathbb{1}_{\mathcal{G}_p}(s),$$

with $\Delta_{p;l}$ denoting the l^{th} element of Δ_p . This enables us to express the cumulant in the form of Lemma S7, as the summands added are all zero, and we have a reference continuous function on \mathbb{R}^d to study, but which when sampled recovers the original taper sequence.

Now for these interpolated functions, for some $1 \leq j \leq t$ write

$$a_{j,n}(s) = \mathcal{I}[\tilde{a}_{j,n}](s).$$

By Proposition S7, we have

$$A_{j,n}(k) = \tilde{A}_{j,n}^{(\mathcal{G})}(k) \prod_{l=1}^d \text{sinc}^2(\pi \Delta_l k_l)$$

where k_l here is the l^{th} element of k . Now

$$\begin{aligned} \tilde{A}_{j,n}^{(\mathcal{G})}(k) &= \left(\prod_{l=1}^d \Delta_l \right) \sum_{s \in \mathcal{G}} \tilde{a}_j(s) e^{-2\pi i k_j \cdot s} \\ &= \left(\prod_{l=1}^d \Delta_l \Delta_{p_j;l} \right) \sum_{s \in \mathcal{G}_{p_j}} h_{m_j,n}(s) e^{-2\pi i k_j \cdot s} \\ &= \left(\prod_{l=1}^d \Delta_l \right) H_{p_j;m_j,n}(k). \end{aligned}$$

All that remains is to check the norms of $A_{j,n}$. In particular, the L_1 norm satisfies

$$\begin{aligned} \int_{\mathbb{R}^d} |A_{j,n}(k)| dk &= \int_{\mathbb{R}^d} \left| H_{p_j;m_j,n}(k) \prod_{l=1}^d \Delta_l \text{sinc}^2(\pi \Delta_l k_l) \right| dk \\ &\leq \sum_{\psi \in \Psi_p} \int_{\mathbb{R}^d} \left| H_{m_j,n}(k + \psi) \prod_{l=1}^d \Delta_l \text{sinc}^2(\pi \Delta_l k_l) \right| dk \\ &= \int_{\mathbb{R}^d} |H_{m_j,n}(k)| \sum_{\psi \in \Psi_p} \prod_{l=1}^d \Delta_l \text{sinc}^2(\pi \Delta_l [k_l - \psi_l]) dk \\ &\leq C_2 \int_{\mathbb{R}^d} |H_{m_j,n}(k)| dk \\ &\rightarrow 0 \end{aligned}$$

as $n \rightarrow 0$. Here C_2 is an upper bound on $\sum_{\psi \in \Psi_p} \prod_{l=1}^d \Delta_l \text{sinc}^2(\pi \Delta_l [k_l - \psi_l])$.

In addition, the L_2 norm satisfies

$$\begin{aligned} \int_{\mathbb{R}^d} |A_{j,n}(k)|^2 dk &= \int_{\mathbb{R}^d} |H_{p_j;m_j,n}(k)|^2 \prod_{l=1}^d \Delta_l^2 \text{sinc}^4(\pi \Delta_l k_l) dk \\ &\leq \sum_{\psi, \psi' \in \Psi_p} \int_{\mathbb{R}^d} \left| H_{m_j,n}(k) \overline{H_{m_j,n}(k + \psi' - \psi)} \right| \prod_{l=1}^d \Delta_l^2 \text{sinc}^4(\pi \Delta_l [k_l - \psi_l]) dk \\ &\leq C_4 \|H_{m_j}\|_2^2 + \left(\|\text{sinc}^4\|_\infty \prod_{l=1}^d \Delta_l^2 \right) \sum_{\psi, \psi' \in \Psi_p} \int_{\mathbb{R}^d} \left| H_{m_j,n}(k) \overline{H_{m_j,n}(k + \psi' - \psi)} \right| dk \\ &\rightarrow C_4 \|H_{m_j}\|_2^2, \end{aligned}$$

as $n \rightarrow \infty$, where C_4 is an upper bound on $\sum_{\psi \in \Psi_p} \prod_{l=1}^d \Delta_l^2 \text{sinc}^4(\pi \Delta_l [k_l - \psi_l])$.

The bounds on the sinc functions exist because we have $\Psi_{p_j} \subseteq \Psi$ due to the grid embedding, and so we need only find a bound for

$$\sum_{\psi \in \Psi} \prod_{l=1}^d \text{sinc}^2(\pi [k_l + \psi_l]) = \prod_{l=1}^d \sum_{z \in \mathbb{Z}} \text{sinc}^2(\pi [\Delta_l k_l + z]).$$

Now in each dimension, by periodicity we have

$$\begin{aligned}
\max_{x \in \mathbb{R}} \sum_{z \in \mathbb{Z}} \text{sinc}^2(\pi[x - z]) &= \max_{x \in [-1/2, 1/2]} \sum_{z \in \mathbb{Z}} \text{sinc}^2(\pi[x - z]) \\
&\leq \sum_{z \in \mathbb{Z}} \max_{x \in [z-1/2, z+1/2]} \text{sinc}^2(\pi x) \\
&= \text{sinc}^2(0) + 2 \sum_{z \in \mathbb{N}} \text{sinc}^2(\pi x - \pi/2) \\
&< \infty
\end{aligned}$$

because $\|\text{sinc}\|_2 < \infty$ and sinc^2 is continuous. The case of sinc^4 is analogous.

Finally, again writing $k'_r = -\sum_{j=1}^{r-1} k'_j$, we have

$$\begin{aligned}
&\mathbb{C}[J_{p_1; m_1, n}(k_1), \dots, J_{p_r; m_r, n}(k_r)] \\
&= \int_{\mathbb{R}^d} \cdots \int_{\mathbb{R}^d} \tilde{f}_{p_1, \dots, p_r}(k'_1, \dots, k'_{r-1}) \prod_{j=1}^r A_{j, n}(k_j - k'_j) dk'_1 \cdots dk'_{r-1} \\
&\leq \|\tilde{f}_{p_1, \dots, p_r}\|_{\infty} \int_{\mathbb{R}^d} \prod_{j=1}^r A_{j, n}(k_j - k'_j) dk'_1 \cdots dk'_{r-1} \\
&= \|\tilde{f}_{p_1, \dots, p_r}\|_{\infty} \int_{\mathbb{R}^d} \left[\prod_{j=1}^{r-1} A_{j, n}(k'_j) \right] A_r \left(\sum_{j=1}^r k_j - \sum_{j=1}^{r-1} k'_j \right) dk'_1 \cdots dk'_{r-1} \\
&= \|\tilde{f}_{p_1, \dots, p_r}\|_{\infty} \tilde{I}_{A, n} \left(\sum_{j=1}^r k_j \right) \\
&\leq \|\tilde{f}_{p_1, \dots, p_r}\|_{\infty} \prod_{j=1}^r \|A_{j, n}\|_{\frac{r}{r-1}} \\
&\leq \|\tilde{f}_{p_1, \dots, p_r}\|_{\infty} \prod_{j=1}^r \left(\|A_{j, n}\|_2^2 \right)^{\frac{1}{r-1}} (\|A_{j, n}\|_1)^{\frac{r-2}{r-1}} \\
&\rightarrow 0.
\end{aligned}$$

Because $A_{j, n}$ satisfies $\|A_{j, n}\|_1 \rightarrow 0$ as $n \rightarrow \infty$. A finite upper bound for $\tilde{f}_{p_1, \dots, p_r}$ is given by $\sum_{u_1 \in \mathcal{G}} \cdots \sum_{u_t \in \mathcal{G}} \int_{\mathbb{R}^d} \cdots \int_{\mathbb{R}^d} |\check{c}_{p_1, \dots, p_r}(u_1, \dots, u_r)| du_{t+1} \cdots du_r < \infty$, which holds by Assumption A1 because $\int_{\mathbb{R}^d} \cdots \int_{\mathbb{R}^d} |\check{c}_{p_1, \dots, p_r}(u_1, \dots, u_r)| du_{t+1} \cdots du_r < \infty$ and $\check{c}_{p_1, \dots, p_r}$ is continuous in the lags related to random fields (the first t). \square

S3 The non-oracle case

Typically when developing the theory of spectral analysis, it is assumed that the process is either mean zero, or that the mean is easily estimated and removed, and so we may act as though the mean is known. We also make this assumption in the theory developed prior to this point, however, it is important to justify this decision. In our case, the mean is often not zero (a simple point process for instance), and so this should be explicitly addressed. Doing no mean removal results in substantial bias, as was noted in the original paper introducing spectra of point processes (Bartlett, 1963). Doing mean removal greatly reduces this bias, as shown by Rajala et al. (2023). However, for finite samples this bias is not completely removed by subtracting the sample mean, though it is greatly reduced in most scenarios. The most extreme case of this is when no taper is applied, and the sample mean used. In this case the tapered Fourier transform is always zero at zero wavenumber. As we will see from the results in this section, in general, the error introduced by not knowing the true intensity/mean can only be large for wavenumbers where $H(k)$ is large (in particular, when doing multitaper estimation, for wavenumbers whose norm is less than the bandwidth).

Say that the intensity (mean) of the process is estimated with a weighted mean, i.e.

$$\hat{\lambda}_p = \int_{\mathbb{R}^d} g_p(u) \xi_p(u)$$

for some function g_p supported on \mathcal{R} satisfying the assumptions of Lemma S1. Studying the mean of the periodogram in this case, we see that the mean is the same as the oracle case, plus some extra error terms.

Proposition S3 (Expectation of the periodogram with unknown mean). *Say that the processes in question satisfy the assumptions of Proposition 2 (the expectation of the periodogram), but that the mean is estimated by a weighted mean as just described. Then*

$$\begin{aligned}\mathbb{E}[I_{p,q;m}(k)] &= \int_{\mathbb{R}^d} H_{p;m}(k-k') \overline{H_{q;m}(k-k')} f_{p,q}(k') dk' \\ &\quad + H_{p;m}(k) \overline{H_{q;m}(k)} (G_p(0) - 1)(G_q(0) - 1) \lambda_p \lambda_q \\ &\quad + H_{p;m}(k) \overline{H_{q;m}(k)} \int_{\mathbb{R}^d} G_p(-k') \overline{G_q(-k')} f_{p,q}(k') dk' \\ &\quad - \overline{H_{q;m}(k)} \int_{\mathbb{R}^d} H_{p;m}(k-k') \overline{G_q(-k')} f_{p,q}(k') dk' \\ &\quad - \overline{H_{q;m}(k)} \int_{\mathbb{R}^d} G_p(-k') \overline{H_{q;m}(k-k')} f_{p,q}(k') dk'\end{aligned}$$

for $k \in \mathbb{R}^d$.

Proof. Write $\xi_p^0(du) = \xi_p(du) - \lambda_p du$. Begin by noting that

$$\hat{\lambda}_p = \int_{\mathbb{R}^d} g_p(u) \xi_p^0(u) + \lambda_p G_p(0).$$

Therefore we can write

$$J_{p;m}(k) = \int_{\mathbb{R}^d} H_{p;m}(u) e^{-2\pi i u \cdot k} \xi_{p0}(du) + H_{p;m}(k) \lambda_p \{1 - G_p(0)\} - H_{p;m}(k) \int_{\mathbb{R}^d} g_p(u) \xi_p^0(du).$$

Terms involving products of the middle term with one of the other in the periodogram will have zero expectation, and so

$$\begin{aligned}\mathbb{E}[I_{p,q;m}(k)] &= \mathbb{E} \left[\int_{\mathbb{R}^d} H_{p;m}(u) e^{-2\pi i u \cdot k} \xi_{0,p}(du) \overline{\int_{\mathbb{R}^d} H_{q;m}(u) e^{-2\pi i u \cdot k} \xi_q^0(du)} \right] \\ &\quad + H_{p;m}(k) \lambda_p (1 - G_p(0)) \overline{H_{q;m}(k) \lambda_q (1 - G_q(0))} \\ &\quad + H_{p;m}(k) \overline{H_{q;m}(k)} \mathbb{E} \left[\int_{\mathbb{R}^d} g_p(u) \xi_p^0(du) \int_{\mathbb{R}^d} g_q(u) \xi_q^0(du) \right] \\ &\quad - \overline{H_{q;m}(k)} \mathbb{E} \left[\int_{\mathbb{R}^d} H_{p;m}(u) e^{-2\pi i u \cdot k} \xi_p^0(du) \int_{\mathbb{R}^d} g_q(u) \xi_q^0(du) \right] \\ &\quad - H_{p;m}(k) \mathbb{E} \left[\int_{\mathbb{R}^d} g_p(u) \xi_p^0(du) \int_{\mathbb{R}^d} H_{q;m}(u) e^{-2\pi i u \cdot k} \xi_q^0(du) \right]\end{aligned}$$

with the remaining terms having zero expectation. All that remains is applying Proposition S1. \square

This is the usual bias, plus terms that scale like the size of the Fourier transform of the taper. Outside of the bandwidth of the taper, this is negligible. If an unbiased estimator of λ is used (for either process), then the second term is zero. The remaining terms are nowhere near the magnitude of bias observed if no mean correction is performed; however, for small samples they may still generate noticeable bias. One approach to address this may be to down weight certain tapers in the multitaper estimator, to remove tapers whose Fourier transform is large at the wavenumber being investigated. Even if this wavenumber is in the bandwidth of the tapers, some of the Fourier transforms will still have little magnitude at this wavenumber (just not all of them). In any case, this issue impacts few wavenumbers, often by negligible amounts in practice.

S4 Linear interpolation

S4.1 Definitions and basic properties

Definition S2. Let \mathcal{I} be the linear interpolation operator, that maps a function of a grid $f : \mathcal{G} \rightarrow \mathbb{R}$ to a function of \mathbb{R}^d by

$$\mathcal{I}[f](u) = \frac{1}{\bar{\Delta}} \sum_{z \in \mathcal{G}} \mathbb{1}_{[0, \Delta)}(u - z) \sum_{v \in \{0, 1\}^d} f(z + v \circ \Delta) \prod_{j=1}^d (u_j - z_j)^{v_j} (\Delta_j - u_j + z_j)^{1-v_j}$$

for any $u \in \mathbb{R}^d$, where $[0, \Delta) = \prod_{j=1}^d [0, \Delta_j)$ and $\bar{\Delta} = \prod_{j=1}^d \Delta_j$.

Definition S3. Let the interpolation weight for a given z and v be

$$\mathcal{I}_{v,z}(u) = \prod_{j=1}^d (u_j - z_j)^{v_j} (\Delta_j - (u_j - z_j))^{1-v_j} \mathbb{1}_{[0, \Delta_j)}(u_j - z_j).$$

Proposition S4. The inner product between a linear interpolation of $g : \mathcal{G} \rightarrow \mathbb{R}^d$ and some other function $h : \mathbb{R}^d \rightarrow \mathbb{R}$ is given by

$$\langle \mathcal{I}[g], h \rangle = \frac{1}{\bar{\Delta}} \sum_{z \in \mathcal{G}} \sum_{v \in \{0, 1\}^d} g(z + v \circ \Delta) \langle h, \mathcal{I}_{v,z} \rangle.$$

Proof. Follows from rearranging the definition and linearity of inner products. \square

Now, many quantities of interest can be derived by considering $\langle h, \mathcal{I}_{v,z} \rangle$ for appropriate choices of h . In particular, in the next two sections, we consider h to be an interpolated function, and then the Fourier basis, so that we can explore the effect on orthogonality and wavenumber domain concentration.

S4.2 Linear interpolation with linear interpolation

Lemma S8. If $v_j, v'_j \in \{0, 1\}$ then

$$\int_0^{\Delta_j} x_j^{v_j+v'_j} (\Delta_j - x_j)^{2-v_j-v'_j} dx_j = \left[(-1)^{v_j+v'_j} \frac{1}{3} + v_j v'_j \right] \Delta_j^3$$

Proof. From the fact that v_j, v'_j are zero or one we have

$$\begin{aligned} & \int_0^{\Delta_j} x_j^{v_j+v'_j} (\Delta_j - x_j)^{2-v_j-v'_j} dx_j \\ &= \int_0^{\Delta_j} \left([1 - v_j] \Delta_j + (-1)^{1-v_j} x_j \right) \left([1 - v'_j] \Delta_j + (-1)^{1-v'_j} x_j \right) dx_j \\ &= \int_0^{\Delta_j} [1 - v_j] [1 - v'_j] \Delta_j^2 + [(-1)^{1-v_j} + (-1)^{1-v'_j}] \Delta_j x_j + (-1)^{2-v_j-v'_j} x_j^2 dx_j \\ &= [1 - v_j] [1 - v'_j] \Delta_j^3 + \frac{(-1)^{1-v_j} + (-1)^{1-v'_j}}{2} \Delta_j^3 + \frac{(-1)^{v_j+v'_j}}{3} \Delta_j^3 \\ &= \begin{cases} \frac{1}{3} \Delta_j^3 & \text{if } v_j = v'_j = 0, \\ \frac{4}{3} \Delta_j^3 & \text{if } v_j = v'_j = 1, \\ -\frac{1}{3} \Delta_j^3 & \text{otherwise.} \end{cases} \end{aligned}$$

\square

Lemma S9. We have that

$$\langle \mathcal{I}_{v',z'}, \mathcal{I}_{v,z} \rangle = \delta_{z,z'} \prod_{j=1}^d \left[(-1)^{v_j+v'_j} \frac{1}{3} + v_j v'_j \right] \Delta_j^3.$$

Proof. From Lemma S8 we see

$$\begin{aligned}\langle \mathcal{I}_{v',z'}, \mathcal{I}_{v,z} \rangle &= \delta_{z,z'} \prod_{j=1}^d \int_0^{\Delta_j} x_j^{v_j+v'_j} (\Delta_j - x_j)^{2-v_j-v'_j} dx_j \\ &= \delta_{z,z'} \prod_{j=1}^d \left[(-1)^{v_j+v'_j} \frac{1}{3} + v_j v'_j \right] \Delta_j^3.\end{aligned}$$

□

Proposition S5. *We have that*

$$\langle \mathcal{I}[g], \mathcal{I}[h] \rangle = \bar{\Delta} \sum_{z \in \mathcal{G}} \sum_{v, v' \in \{0,1\}^d} g(z + v \circ \Delta) h(z + v' \circ \Delta) \prod_{j=1}^d \left[(-1)^{v_j+v'_j} \frac{1}{3} + v_j v'_j \right].$$

Proof. Using Lemma S9 and Proposition S4

$$\begin{aligned}\langle \mathcal{I}[g], \mathcal{I}[h] \rangle &= \frac{1}{\bar{\Delta}} \sum_{z \in \mathcal{G}} \sum_{v \in \{0,1\}^d} g(z + v \circ \Delta) \langle \mathcal{I}[h], \mathcal{I}_{v,z} \rangle \\ &= \frac{1}{\bar{\Delta}^2} \sum_{z \in \mathcal{G}} \sum_{v, v' \in \{0,1\}^d} g(z + v \circ \Delta) h(z + v' \circ \Delta) \prod_{j=1}^d \left[(-1)^{v_j+v'_j} \frac{1}{3} + v_j v'_j \right] \Delta_j^3\end{aligned}$$

□

Now we can rescale the interpolated tapers to have and L_2 norm of one, and use this to check the cross inner products are still close to zero. If they are not, we can fix this by increasing the grid resolution, as demonstrated in the next proposition.

Proposition S6. *Let $g, h : \mathcal{G} \rightarrow \mathbb{R}$, then*

$$\langle \mathcal{I}[g], \mathcal{I}[h] \rangle = \bar{\Delta} \langle g, h \rangle + \bar{\Delta} \epsilon,$$

where

$$|\epsilon| \leq \|g\|_1 \max_{v \in \{0,1\}^d} \max_{z \in \mathcal{G}} |h(z + v \circ \Delta) - h(z)| + \|h\|_1 \max_{v \in \{0,1\}^d} \max_{z \in \mathcal{G}} |g(z + v \circ \Delta) - g(z)|.$$

Proof. Using Proposition S5 we have

$$\begin{aligned}\langle \mathcal{I}[g], \mathcal{I}[h] \rangle &= \bar{\Delta} \sum_{z \in \mathcal{G}} \sum_{v, v' \in \{0,1\}^d} g(z + v \circ \Delta) h(z + v' \circ \Delta) \prod_{j=1}^d \left[(-1)^{v_j+v'_j} \frac{1}{3} + v_j v'_j \right] \\ &= \bar{\Delta} \sum_{z \in \mathcal{G}} g(z) h(z) \sum_{v, v' \in \{0,1\}^d} \prod_{j=1}^d \left[(-1)^{v_j+v'_j} \frac{1}{3} + v_j v'_j \right] + \epsilon \\ &= \bar{\Delta} \langle g, h \rangle \prod_{j=1}^d [1/3 - 1/3 - 1/3 + 4/3] + \bar{\Delta} \epsilon \\ &= \bar{\Delta} \langle g, h \rangle + \bar{\Delta} \epsilon,\end{aligned}$$

where

$$\epsilon = \epsilon_1 + \epsilon_2,$$

$$\epsilon_1 = \sum_{z \in \mathcal{G}} \sum_{v, v' \in \{0,1\}^d} [g(z + v \circ \Delta) - g(z)] h(z + v' \circ \Delta) \prod_{j=1}^d \left[(-1)^{v_j+v'_j} \frac{1}{3} + v_j v'_j \right],$$

$$\epsilon_2 = \sum_{z \in \mathcal{G}} \sum_{v, v' \in \{0,1\}^d} [h(z + v' \circ \Delta) - h(z)] g(z) \prod_{j=1}^d \left[(-1)^{v_j+v'_j} \frac{1}{3} + v_j v'_j \right].$$

Then we have a bound

$$\begin{aligned}
|\epsilon_1| &\leq \sum_{z \in \mathcal{G}} \sum_{v, v' \in \{0,1\}^d} h(z + v' \circ \Delta) \prod_{j=1}^d \left[(-1)^{v_j + v'_j} \frac{1}{3} + v_j v'_j \right] \max_{v \in \{0,1\}^d} \max_{z \in \mathcal{G}} |h(z + v \circ \Delta) - h(z)| \\
&= \left(\sum_{z \in \mathcal{G}} \sum_{v' \in \{0,1\}^d} h(z + v' \circ \Delta) \prod_{j=1}^d v'_j \right) \max_{v \in \{0,1\}^d} \max_{z \in \mathcal{G}} |h(z + v \circ \Delta) - h(z)| \\
&= \|g\|_1 \max_{v \in \{0,1\}^d} \max_{z \in \mathcal{G}} |h(z + v \circ \Delta) - h(z)|,
\end{aligned}$$

similarly

$$|\epsilon_2| \leq \|h\|_1 \max_{v \in \{0,1\}^d} \max_{z \in \mathcal{G}} |g(z + v \circ \Delta) - g(z)|,$$

the stated bound follows from combining the two. \square

In other words, it is the change in g and h between consecutive grid points that causes the error in the inner product. This will typically be small due to the assumption that the Fourier transforms of h and g are concentrated at low wavenumbers, but this can be reduced by increasing the grid resolution.

S4.3 Linear interpolation with Fourier basis

The following proposition tells us how to calculate the Fourier transform of a linearly interpolated taper, which we will require for mean removal of the point patterns, and for examining the quality of our tapers.

Proposition S7. *Let $\phi_k(u) = e^{-2\pi i u \cdot k}$ and $g : \mathcal{G} \rightarrow \mathbb{R}$ then*

$$\langle \mathcal{I}[g], \phi_k \rangle = G^{(\mathcal{G})}(k) \prod_{j=1}^d \text{sinc}^2(\pi \Delta_j k_j)$$

where k_j is the j^{th} element of k .

Proof. Firstly, notice that

$$\begin{aligned}
\langle \phi_k, \mathcal{I}_{v,z} \rangle e^{2\pi i(z+v \circ \Delta) \cdot k} &= e^{2\pi i(z+v \circ \Delta) \cdot k} \prod_{j=1}^d \int_0^{\Delta_j} x_j^{v_j} (\Delta_j - x_j)^{1-v_j} e^{-2\pi i k_j (x_j + z_j)} dx_j \\
&= \prod_{j=1}^d \int_0^{\Delta_j} x_j^{v_j} (\Delta_j - x_j)^{1-v_j} e^{-2\pi i k_j (x_j - v_j \Delta_j)} dx_j,
\end{aligned}$$

is invariant to z . Therefore

$$\begin{aligned}
\langle \mathcal{I}[g], \phi_k \rangle &= \frac{1}{\Delta} \sum_{z \in \mathcal{G}} \sum_{v \in \{0,1\}^d} g(z + v \circ \Delta) \langle \phi_k, \mathcal{I}_{v,z} \rangle \\
&= \frac{1}{\Delta} \sum_{v \in \{0,1\}^d} \left(\sum_{z \in \mathcal{G}} g(z + v \circ \Delta) e^{-2\pi i(z+v \circ \Delta) \cdot k} \right) \langle \phi_k, \mathcal{I}_{v,z} \rangle e^{2\pi i(z+v \circ \Delta) \cdot k} \\
&= \frac{1}{\Delta^2} G^{(\mathcal{G})}(k) \sum_{v \in \{0,1\}^d} \langle \phi_k, \mathcal{I}_{v,z} \rangle e^{2\pi i(z+v \circ \Delta) \cdot k}.
\end{aligned}$$

Now we have

$$\begin{aligned}
\sum_{v \in \{0,1\}^d} \langle \phi_k, \mathcal{I}_{v,z} \rangle e^{2\pi i(z+v \circ \Delta) \cdot k} &= \sum_{v \in \{0,1\}^d} \prod_{j=1}^d \int_0^{\Delta_j} x_j^{v_j} (\Delta_j - x_j)^{1-v_j} e^{-2\pi i k_j (x_j - v_j \Delta_j)} dx_j \\
&= \prod_{j=1}^d \sum_{v=0}^1 \int_0^{\Delta_j} x_j^{v_j} (\Delta_j - x_j)^{1-v_j} e^{-2\pi i k_j (x_j - v_j \Delta_j)} dx_j \\
&= \prod_{j=1}^d \int_0^{\Delta_j} (\Delta_j - x_j) e^{-2\pi i k_j x_j} + x_j e^{-2\pi i k_j (x_j - \Delta_j)} dx_j \\
&= \prod_{j=1}^d \text{sinc}^2(\pi \Delta_j k_j) \Delta_j^2,
\end{aligned}$$

because if $k_j \neq 0$

$$\begin{aligned}
&\int_0^{\Delta_j} (\Delta_j - x_j) e^{-2\pi i k_j x_j} + x_j e^{-2\pi i k_j (x_j - \Delta_j)} dx_j \\
&= \int_0^{\Delta_j} (\Delta_j - x_j) e^{-2\pi i k_j x_j} dx_j + \int_0^{\Delta_j} (\Delta_j - x_j) e^{2\pi i k_j x_j} dx_j \\
&= 2 \operatorname{Re} \left\{ \int_0^{\Delta_j} (\Delta_j - x_j) e^{2\pi i k_j x_j} dx_j \right\} \\
&= 2 \operatorname{Re} \left\{ \frac{2\pi i \Delta_j k_j - e^{2\pi i \Delta_j k_j} + 1}{2\pi^2 k_j^2} \right\} \\
&= \frac{\sin^2(\pi \Delta_j k_j)}{\pi^2 k_j^2},
\end{aligned}$$

otherwise if $k_j = 0$,

$$\int_0^{\Delta_j} (\Delta_j - x_j) e^{-2\pi i k_j x_j} + x_j e^{-2\pi i k_j (x_j - \Delta_j)} dx_j = \int_0^{\Delta_j} \Delta_j dx_j = \Delta_j^2.$$

The stated result follows. \square

In practice, we scale the function g such that $\|\mathcal{I}[g]\|_2 = 1$.

S5 Bias in marked point processes

S5.1 The expectation of the biased periodogram

Periodograms have been proposed for marked point processes, both in the univariate (Renshaw, 2002) and multivariate (Eckardt and Mateu, 2019a) cases, however, these estimators are unfortunately systematically biased. Without loss of generality, consider the univariate case, where X is the point locations and $W(x)$ is the mark at that location. We call this process the marked process, and the point process without the marks the ground process (Daley and Vere-Jones, 2003). Breaking slightly from our previous notation, write λ_g for the intensity of the ground process, λ_m for the intensity of the marked process, and μ for the mean of the marks. (Renshaw, 2002) write an alternate discrete Fourier transform for the marked case as

$$\mathfrak{F}(k) = \frac{1}{\sqrt{\ell(\mathcal{R})}} \sum_{x \in X \cap \mathcal{R}} (W(x) - \mu) e^{-2\pi i x k}.$$

Renshaw (2002) only define this for rectangular regions but for convenience we study the general case here. The proposed periodogram is then $|\mathfrak{F}(k)|^2$.

Denote the discrete Fourier transform of the ground process (using only the points) and marked process by

$$J_g(k) = \frac{1}{\sqrt{\ell(\mathcal{R})}} \sum_{x \in X \cap \mathcal{R}} e^{-2\pi i x k} - \lambda_g \int_{\mathcal{R}} e^{-2\pi i x k} dx,$$

$$J_m(k) = \frac{1}{\sqrt{\ell(\mathcal{R})}} \sum_{x \in X \cap \mathcal{R}} M(x) e^{-2\pi i x k} - \lambda_m \int_{\mathcal{R}} e^{-2\pi i x k} dx,$$

respectively. The mean correction we propose is different to that of Renshaw (2002) in that we subtract λ_m not μ , and we do this everywhere, not just at the atoms of the mark sum measure. In any case, $\lambda_m = \mu\lambda_g$ (Illian et al., 2008, equation 5.1.19), and so

$$\begin{aligned} \mathfrak{F}(k) &= \frac{1}{\sqrt{\ell(\mathcal{R})}} \sum_{x \in X \cap \mathcal{R}} (M(x) - \mu) e^{-2\pi i x k} \\ &= \frac{1}{\sqrt{\ell(\mathcal{R})}} \sum_{x \in X \cap \mathcal{R}} M(x) e^{-2\pi i x k} - \lambda_m H(k) - \mu \left[\frac{1}{\sqrt{\ell(\mathcal{R})}} \sum_{x \in X \cap \mathcal{R}} e^{-2\pi i x k} - \lambda_g H(k) \right] \\ &= J_m(k) - \mu J_g(k), \end{aligned}$$

where for convenience we define

$$H(k) = \int_{\mathcal{R}} \frac{1}{\sqrt{\ell(\mathcal{R})}} e^{-2\pi i x k} dx.$$

Therefore

$$\begin{aligned} |\mathfrak{F}(k)|^2 &= I_{mm}(k) + \mu^2 I_{gg}(k) - 2\mu \operatorname{Re}\{I_{mg}(k)\} \\ &\rightarrow f_{mm}(k) + \mu^2 f_{gg}(k) - 2\mu \operatorname{Re}\{f_{mg}(k)\}, \end{aligned}$$

as the region grows. This does not equal $f_{mm}(k)$, our desired estimand.

S5.2 The definition of spectra for marked processes

In fact, the definition of the spectral density function given in Renshaw (2002) and Eckardt and Mateu (2019a) is not the same as the definition we use in this paper. However, it is not equal to $f_{mm}(k) + \mu^2 f_{gg}(k) - 2\mu \operatorname{Re}\{f_{mg}(k)\}$. In particular, Renshaw (2002) define the spectral density function as the Fourier transform of the reduced factorial moment measure of the mark sum measure (though it is written differently in the paper, it is equivalent). In contrast, we Fourier transform the reduced cumulant measure, matching the definition for point processes, random fields and general random measures (Daley and Vere-Jones, 2003). In particular, define

- λ_g : the intensity of the ground process
- μ : the mean of the mark (conditional on a point existing)
- $\lambda_m = \lambda_g \mu$: the mark intensity
- μ_2 : the second moment of the mark (conditional on a point)
- ρ_{gg}, ρ_{mm} : the second-order product density of the ground process and mark sum measure respectively (factorial moment density)
- \check{c}_m : the complete covariance of the ground process and the mark sum measure respectively
- $k_{mm}(x) = \rho_{mm}(x) / \rho_{gg}(x) \mu^2$: the mark correlation, note this definition is from Eckardt and Mateu (2019b) and Illian et al. (2008), who divide by μ^2 . Eckardt and Mateu (2019a) only divide by μ , though this doesn't impact the point of what follows.

Define the mean product of marks as

$$\begin{aligned} U(x) &= \rho_{gg}(x) k_{mm}(x) \\ &= \rho_{mm}(x) \frac{1}{\mu^2} \end{aligned}$$

Then Renshaw (2002) define the spectra to be

$$S(k) = \int_{\mathbb{R}^d} U(x) e^{2\pi i k \cdot x} dx.$$

In contrast, the spectral density function of the mark sum measure is given by

$$f_m(k) = \int_{\mathbb{R}^d} \check{c}_m(x) e^{2\pi i k \cdot x} dx$$

where

$$\check{c}_m(x) = \rho_{mm}(x) - \lambda_m^2 + \lambda_g \mu_2 \delta(x)$$

this can be found from Proposition 8.1.IV of Daley and Vere-Jones (2003).

We can therefore relate the two spectra from

$$U(x) = \frac{1}{\mu^2} (\check{c}_m(x) + \lambda_m^2 - \lambda_g \mu_2 \delta(x))$$

and so

$$S_m(k) = \frac{1}{\mu^2} (f_m(k) + \lambda_m^2 \delta(k) - \lambda_g \mu_2).$$

Notice that one of the two spectra will not be a function in the usual sense. Consider the case when the ground point process has a spectral density f_g , and the marks are independent of the ground process and are IID, then the ground and mark spectra are related by

$$f_m(k) = \mu_1^2 f_g(k) + \lambda_g (\mu_2 - \mu^2)$$

(Daley and Vere-Jones, 2003). So in this case, our definition of spectral density function is a density, whilst the Renshaw spectra is not. Furthermore, if we set the marks to have a point mass at 1, we obtain $\mu_2 = \mu = 1$, and so

$$f_m(k) = f_g(k)$$

as one would expect. Again this is not true of Renshaw spectra.

Whilst this is a choice, it is sensible to choose the cumulant measure to Fourier transform, a choice which is made in the point process case, even in Renshaw (2002). Consider a basic null model where we have multiple independent Poisson processes with IID marks. Under the definition of Renshaw (2002) and Eckardt and Mateu (2019a), the spectral density matrix function would be zero (except for a point mass at zero). This means that the spectral density matrix is not invertible at most frequencies, and thus partial coherence would not be well define even in the most simple case, in contrast to our definition. Furthermore, our definition is an exact generalisation of the unmarked case, as setting the marks to a point mass at one recovers the unmarked case, both in the spectral density function and our proposed estimators.

S5.3 Small simulation study

To verify the bias in the alternate periodogram, we performed a small simulation study. We simulate Poisson processes with intensity $\lambda = 0.001$, with marks drawn from an IID Normal(1.5,0.4) distribution. We generate 1000 replications and at each estimate the spectra with multitapering and the alternate periodogram. We show a comparison of the true spectra to two estimates in Fig. 6. To ease comparison, we take a slice at $k_2 = 0$. We can see that indeed the existing methodology is significantly biased, but the multitaper estimator is not.

S6 Additional details from the main simulation study

In the following models, we always have one random field and two point processes. In each case, the random field is a log-Gaussian process, where the Gaussian process had mean -6 and a Matérn covariance function with length scale 20m, smoothness 3 and variance 1. The specific details of the three models considered in the paper are as follows:

- Model 1: The two point processes are independent log-Gaussian Cox processes with the Gaussian process described above driving them (independently of the recorded random field).
- Model 2: The two point processes are independently Cox processes with the random intensity driven by the field (i.e. they are log-Gaussian Cox processes, see Møller et al. (1998)).
- Model 3: The second point process is a log-Gaussian Cox process with the random intensity driven by the field, and the first point process is the result of random clustering around the second point process, where for each point in the first process, there are Poisson(1) children, who are placed randomly around the parent with a Normal(0, 5²) distribution in each direction.

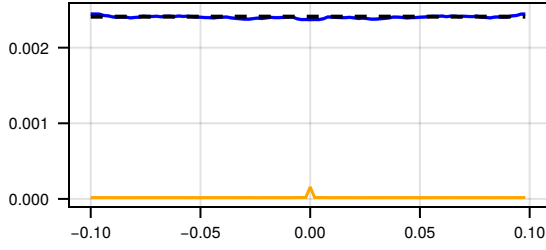


Figure 6: The true spectral density function of the IID marked Poisson process (dashed), the average of the multitaper estimates (blue) and the average of the alternate periodogram (orange). Taken at the slice $k_2 = 0$.

In each case, the random field is recorded on a grid with spacing every 5m starting from (0m,0m) as in the case of the gradient data from Barro Colorado Island.

Say that the p^{th} process is a log-Gaussian random field, and the q^{th} and r^{th} processes are point processes which are conditionally inhomogeneous Poisson processes with rate function $Y_p(s)$, but which are conditionally independent of each other. Let c be the covariance function of the Gaussian random field, from Møller et al. (1998) we have

$$\lambda_q = e^{\lambda_p + c(0)/2}$$

$$\check{c}_{q,q}(u) = (\lambda_q)^2 [e^{c(u)} - 1] + \lambda_q \delta(u).$$

By similar arguments one also has

$$\check{c}_{q,p}(u) = (\lambda_q)^2 [e^{c(u)} - 1]$$

$$\check{c}_{q,r}(u) = (\lambda_q)^2 [e^{c(u)} - 1]$$

In the wavenumber domain, the spectral density functions are therefore

$$f_{q,q}(k) = (\lambda_q)^2 \int_{\mathbb{R}^d} (e^{c(u)} - 1) e^{-2\pi i u \cdot k} du + \lambda_q,$$

$$f_{p,q}(k) = (\lambda_q)^2 \int_{\mathbb{R}^d} (e^{c(u)} - 1) e^{-2\pi i u \cdot k} du,$$

$$f_{p,r}(k) = (\lambda_q)^2 \int_{\mathbb{R}^d} (e^{c(u)} - 1) e^{-2\pi i u \cdot k} du.$$

For the final model, we approximate the true spectral density function through simulations.

Example realizations and corresponding spectral estimates for models 2 and 3 are shown in Fig. 7. We can see that the estimated spectra do a good job of reflecting the underlying structure of the model from which the data was simulated. The results of the simulation study when the swamp is included is shown in Fig. 8. Again as was the case when the swamp was removed, the theoretical distributions are relatively close to the empirical results, further justifying the use of the asymptotic distributions in the main paper.

S7 Additional simulation models and results

S7.1 Colocation model

Consider a multivariate random field model, in particular, a colocation model, see Waagepetersen et al. (2016) for a description. In our case, we consider one shared latent field, and two individual fields, so that the output fields are given by

$$Y_1(s) = U_1(s) + \alpha_1 X(s),$$

$$Y_2(s) = U_2(s) + \alpha_2 X(s),$$

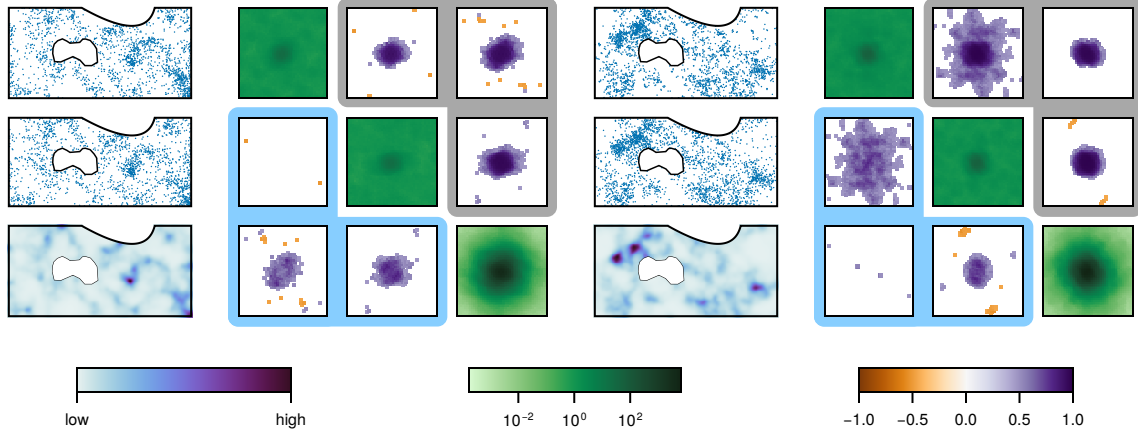


Figure 7: A realization of models 2 (left) and 3 (right). The spatial data has axes 0 to 1000 and 0 to 500, and the wavenumber domain plots show both k_1 and k_2 ranging from -0.05 to 0.05. Colorbars indicate from left to right, the value of the field from low to high, the value of the log standardized marginal spectra and the value of the signed coherence and signed partial coherence. In both cases, the swamp is excluded.

for some $\alpha_1, \alpha_2 \in \mathbb{R}$. In our case, the random fields U_1, U_2, X are all assumed to be independent of each other. In this case, we have that for $1 \leq p, q \leq 2$,

$$f_{p,q}^{(Y)}(k) = f_{p,q}^{(U)}(k)\delta_{p,q} + \alpha_p\alpha_q f^{(X)}(k),$$

where subscripts indicate the spectrum corresponds to that kind of process.

Furthermore, we assume the processes U_1, U_2, X are Gaussian with the same marginal covariance structure, but we choose different grids for the sampling two processes Y_1 and Y_2 . Recall the grid for the j^{th} process is specified by its spatial offset v_j , and sampling interval Δ_j , which in this case are both in \mathbb{R}^2 . In particular,

The grids are defined by

$$\begin{aligned} v_1 &= (0, 0), & \Delta_1 &= (5, 5), \\ v_2 &= (0, 3), & \Delta_2 &= (10, 15). \end{aligned}$$

And the covariance function is Matérn, with length scale $\ell = 20$ and smoothness parameter $\nu = 3$ (and variance $\sigma = 1.0$). We take $\alpha_1 = 0.8$ and $\alpha_2 = 0.5$.

We run the simulation 1000 times. We show the average of the log spectrum, and the coherence and group delay in Fig. 9. The average estimate is close to the true value, and the estimate from a single realization is also close to the true value. However, as expected we can see the effect of aliasing in the second process, as that grid is courser.

S7.2 Shifted point pattern

Say that we have some initial point pattern ξ_p , whose covariance has no atoms other than at zero. Construct ξ_q by shifting every point in the original pattern by some fixed $\tau \in \mathbb{R}^d \setminus \{0\}$, i.e. so that $\xi_q(B) = \xi_p(B - \tau)$. Then there is an atom present in the cross-covariance (though it is not at zero), in particular

$$\check{c}_{p,q}(u) = \lambda_p \delta(u + \tau) + \check{c}_{[p,p]}(u + \tau) = \check{c}_{p,p}(u + \tau), \quad u \in \mathbb{R}^d,$$

where $\check{c}_{[p,p]}$ is the factorial covariance density of the point process ξ_p . Thus the cross-spectral density function is given by

$$\begin{aligned} f_{p,q}(k) &= \int_{\mathbb{R}^d} \check{c}_{p,p}(u + \tau) e^{-2\pi i u \cdot k} du \\ &= f_{p,p}(k) e^{2\pi i \tau \cdot k}, \end{aligned}$$

for $k \in \mathbb{R}^d$.

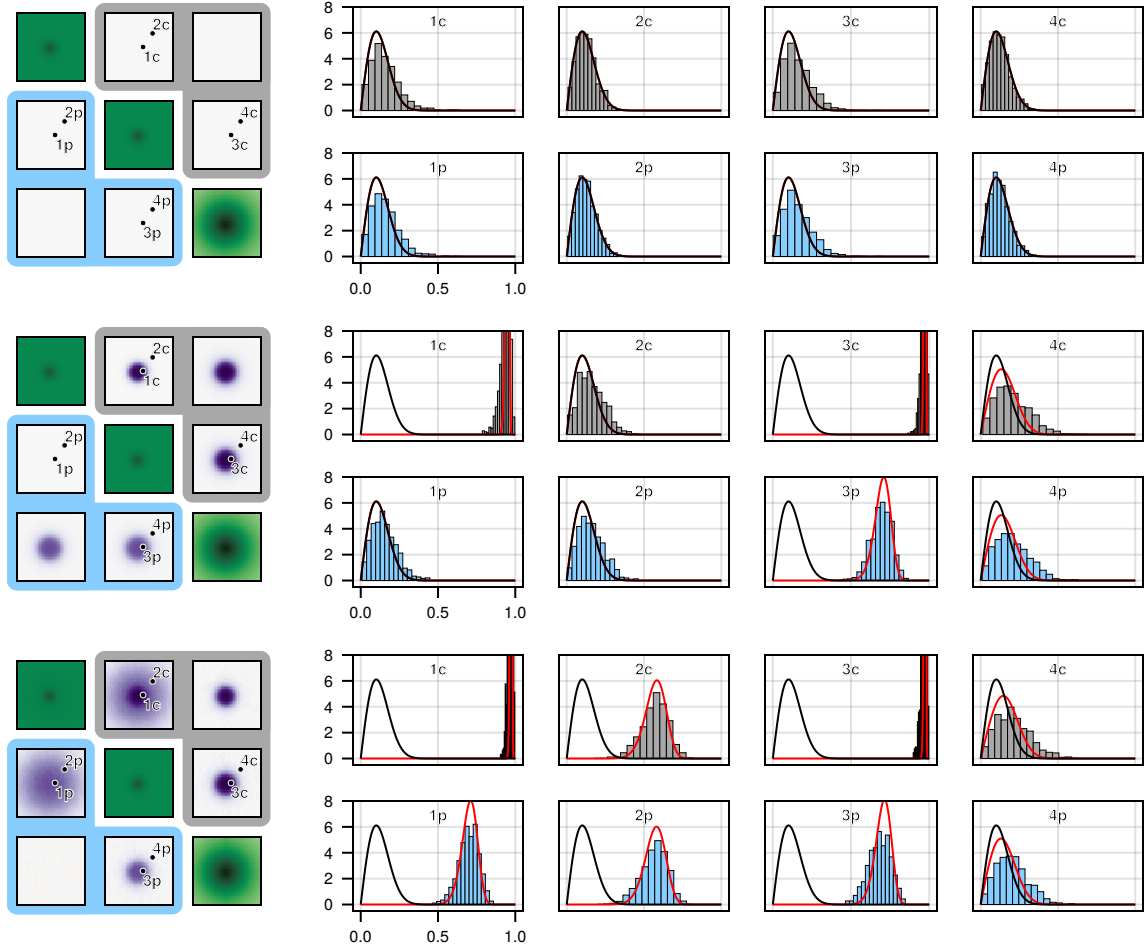


Figure 8: Results of the simulation study with the swamp included. The left column shows the true spectral matrix for each model, with the magnitude coherence in the upper triangle and magnitude partial coherence in the lower triangle where both k_1 and k_2 range from -0.05 to 0.05 . The right hand column shows the estimated magnitude coherence and magnitude partial coherence vs asymptotic distribution (red line) and asymptotic null distribution (black line). Each of the three rows corresponds to a different model (the figures have been truncated where appropriate).

Though not a realistic process, this shifted example is still important as these simple cases are helpful for developing intuition about the cross-spectral density function and related quantities. In particular, the two processes in question have perfect coherence, but with some fixed group delay. In the time series case, taking a process and its deterministic shift, we also have perfect coherence and some group delay determined by the shift. As in the time series case, such examples allow us to build intuition about group delay in terms of spatial shifts.

Consider a Poisson process with intensity $\lambda = 0.001$, and then make a second by shifting the first by $(10.5, 15)$, again performing 1000 replications. The average vs true log marginal spectra, coherence and group delay are shown in Fig. 10. We see that as in the theory, the estimate obtains a constant coherence with a group delay which is linear, though it is plotted modulus 2π on the interval $(-\pi, \pi]$.

S7.3 Partial correlation of normal random variables

We use the distribution of magnitude correlation for magnitude partial correlation of normal random variables in the paper. To examine this, we consider a simple simulation experiment. In particular, define

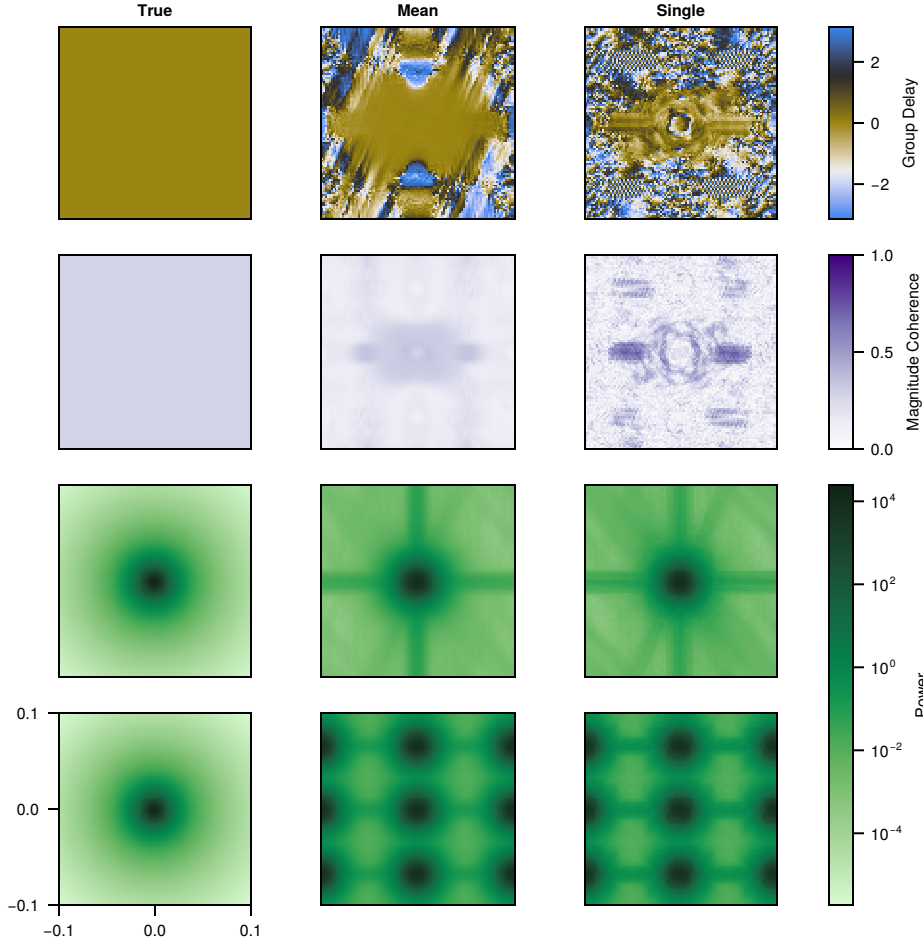


Figure 9: The log marginal spectra, coherence and group delay for the colocation model. In each case, we show and the ground truth (left), the average over 1000 replications (middle) and the estimate from a single realization (right). In the case of group delay, the average estimate uses a circular average.

$$\begin{aligned}
 z &\sim \mathcal{CN}(0, 1, 0) \\
 \epsilon &\sim \mathcal{CN}(0, 1, 0) \\
 \nu &\sim \mathcal{CN}(0, 1, 0) \\
 \eta &= \rho\epsilon + (1 - \rho^2)^{1/2}\nu \\
 x &= z + \epsilon\sigma \\
 y &= z + \eta\sigma
 \end{aligned}$$

and consider the correlation of x and y , and the partial correlation of x and y given z . Assume that we obtain n replications of x, y, z . We compute the sample magnitude correlation and partial magnitude correlation for a range of ρ in simulations (assuming the mean is known to be zero and fixing $\sigma = 1$). We perform this experiment 10000 times for each value of ρ and multiple values of n . We show the results in Fig. 11. Note that except for very small n , the distributional approximation is very good for the partial magnitude correlation (of course it is exact for magnitude correlation).

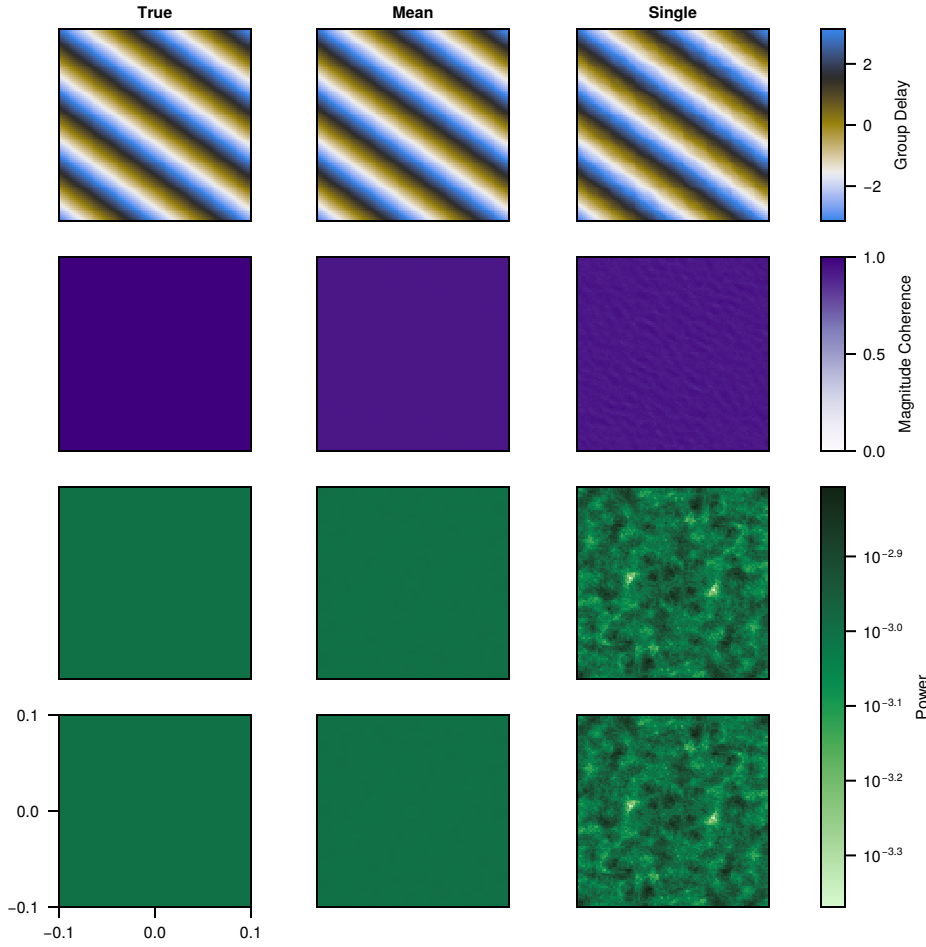


Figure 10: The log marginal spectra, coherence and group delay for the shifted model. In each case, we show and the ground truth (left), the average over 1000 replications (middle) and the estimate from a single realization (right). In the case of group delay, the average estimate uses a circular average.

S8 Additional application figures

The group delay for the Barro Colorado Island data for the first analysis (*Beilschmiedia towarensis*, *Poulsenia armata* and gradient) is shown in Fig. 12, and for the second analysis (*Tabebuia rosea* and the level of Manganese and Phosphorus) is shown in Fig. 13. We see that for large values of the marginal spectra, they are close to zero or π , as expected.

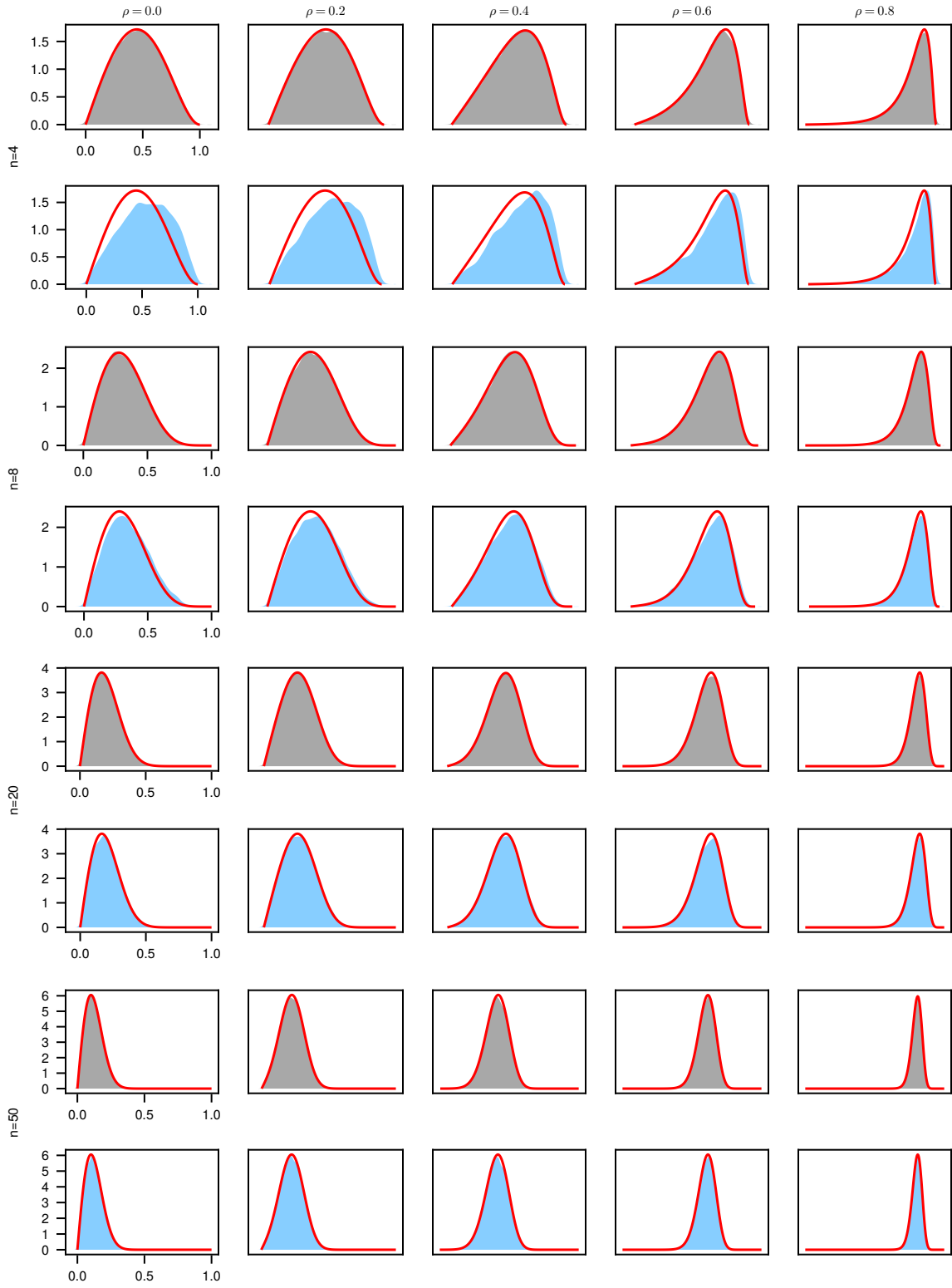


Figure 11: The empirical distributions of the magnitude correlation and partial magnitude correlation for normal random variables vs the truth (shown by the red line). Rows are organized so they alternate correlation (gray) and partial correlation (blue).

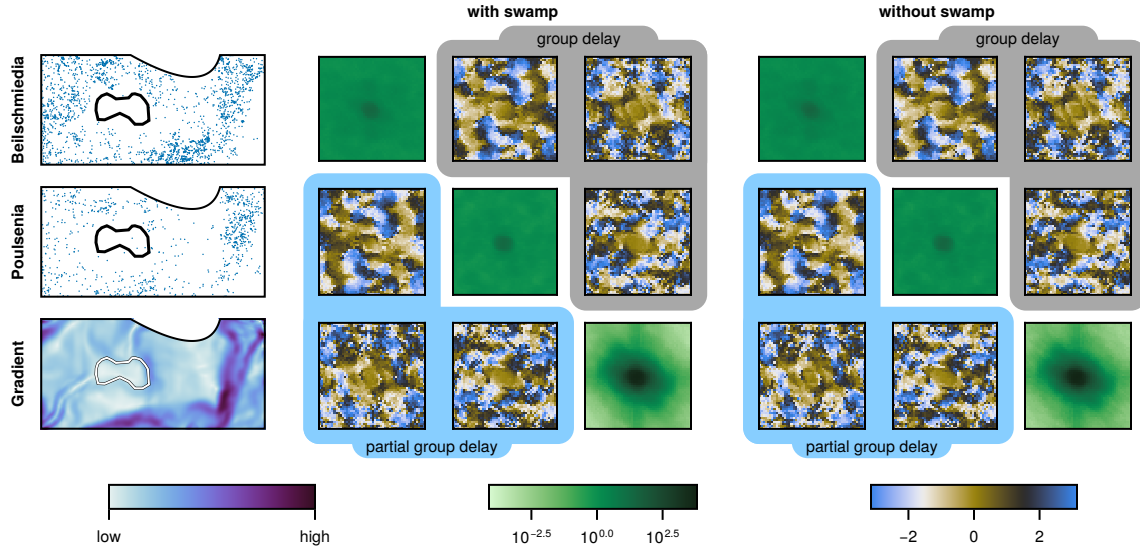


Figure 12: Group delay *Beilschmiedia tovarensis*, *Poulsenia armata* and the gradient of the terrain. The spatial data has axes 0 to 1000 and 0 to 500, and the wavenumber domain plots show both k_1 and k_2 ranging from -0.05 to 0.05. Colorbars indicate from left to right, the value of the field from low to high, the value of the log standardized marginal spectra and the value of the group delay and partial group delay.

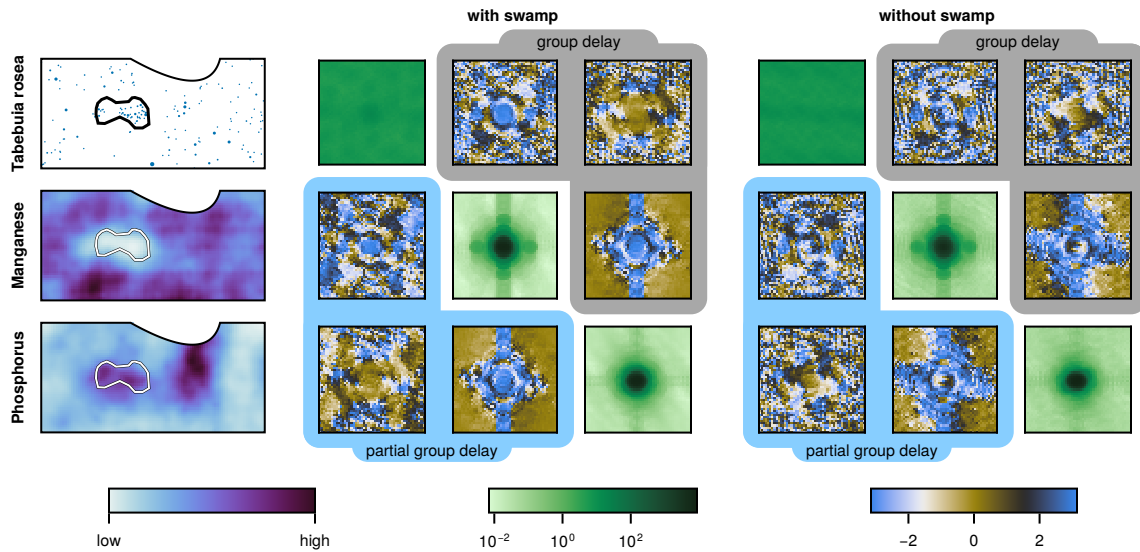


Figure 13: Group delay for the growth of *Tabebuia rosea* and the level of Manganese and Phosphorus in the soil. The format is as in Fig. 12.

References

- Adler, R. J. (2010). *The Geometry of Random Fields*. SIAM.
- Andén, J. and Romero, J. L. (2020). Multitaper estimation on arbitrary domains. *SIAM Journal on Imaging Sciences*, 13(3):1565–1594.
- Astfalck, L. C., Sykulski, A. M., and Cripps, E. J. (2024). Debiasing Welch’s method for spectral density estimation. *Biometrika*, page asae033.
- Baddeley, A., Rubak, E., and Turner, R. (2015). *Spatial Point Patterns: Methodology and Applications with R*. Chapman and Hall/CRC Press, London.
- Bandyopadhyay, S. and Lahiri, S. N. (2009). Asymptotic properties of discrete Fourier transforms for spatial data. *Sankhyā: The Indian Journal of Statistics, Series A*, pages 221–259.
- Barnett, A. H., Magland, J., and af Klinteberg, L. (2019). A parallel nonuniform fast Fourier transform library based on an “exponential of semicircle” kernel. *SIAM Journal on Scientific Computing*, 41(5):C479–C504.
- Bartlett, M. S. (1963). The spectral analysis of point processes. *Journal of the Royal Statistical Society Series B: Statistical Methodology*, 25(2):264–281.
- Bartlett, M. S. (1964). The spectral analysis of two-dimensional point processes. *Biometrika*, 51(3/4):299–311.
- Bonferroni, C. (1936). Teoria statistica delle classi e calcolo delle probabilita. *Pubblicazioni del R istituto superiore di scienze economiche e commerciali di firenze*, 8:3–62.
- Brillinger, D. (1972). The spectral analysis of stationary interval functions. *Proceedings of the 6th Berkeley Symposium on Mathematical Statistics and Probability*, 1.
- Brillinger, D. R. (1974). *Time Series: Data Analysis and Theory*. International series in decision processes. Holt, Rinehart, and Winston, New York.
- Brillinger, D. R. (1982). Asymptotic normality of finite Fourier transforms of stationary generalized processes. *J. Multivariate Anal.*, 12(1):64–71.
- Carter, G., Knapp, C., and Nuttall, A. (1973). Statistics of the estimate of the magnitude-coherence function. *IEEE transactions on audio and electroacoustics*, 21(4):388–389.
- Carter, G. C. (1987). Coherence and time delay estimation. *Proceedings of the IEEE*, 75(2):236–255.
- Condit, R., Pérez, R., Aguilar, S., Lao, S., Foster, R., and Hubbell, S. (2019). Complete data from the Barro Colorado 50-ha plot: 423617 trees, 35 years.
- Cooley, J. W. and Tukey, J. W. (1965). An algorithm for the machine calculation of complex Fourier series. *Mathematics of computation*, 19(90):297–301.
- Dahlhaus, R. (2000). Graphical interaction models for multivariate time series. *Metrika*, 51:157–172.
- Daley, D. J. and Vere-Jones, D. (2003). *An Introduction to the Theory of Point Processes, Volume I: Elementary Theory and Methods*. Springer.
- Diggle, P. J., Gates, D. J., and Stibbard, A. (1987). A nonparametric estimator for pairwise-interaction point processes. *Biometrika*, 74(4):763–770.
- Dutt, A. and Rokhlin, V. (1993). Fast Fourier transforms for nonequispaced data. *SIAM Journal on Scientific computing*, 14(6):1368–1393.
- Eckardt, M. and Mateu, J. (2019a). Analysing multivariate spatial point processes with continuous marks: A graphical modelling approach. *International Statistical Review*, 87(1):44–67.
- Eckardt, M. and Mateu, J. (2019b). Partial characteristics for marked spatial point processes. *Environmetrics*, 30(6):e2565.
- Eckardt, M. and Mateu, J. (2019c). A spatial dependence graph model for multivariate spatial hybrid processes. *arXiv preprint arXiv:1906.07798*.
- Flügge, A. J., Olhede, S. C., and Murrell, D. J. (2014). A method to detect subcommunities from multivariate spatial associations. *Methods in Ecology and Evolution*, 5(11):1214–1224.
- Foy, C., Chaney, R. t., and White, M. (1978). The physiology of metal toxicity in plants. *Annual review of plant physiology*, 29(1):511–566.
- Goodman, N. R. (1957). *On the Joint Estimation of the Spectra, Cospectrum and Quadrature Spectrum of a Two-Dimensional Stationary Gaussian Process*. Princeton University.

- Guillaumin, A. P., Sykulski, A. M., Olhede, S. C., and Simons, F. J. (2022). The debiased spatial Whittle likelihood. *Journal of the Royal Statistical Society Series B: Statistical Methodology*, 84(4):1526–1557.
- Harms, K. E., Condit, R., Hubbell, S. P., and Foster, R. B. (2001). Habitat associations of trees and shrubs in a 50-ha neotropical forest plot. *Journal of ecology*, 89(6):947–959.
- Hubbell, S. P. and Foster, R. B. (1983). Diversity of canopy trees in a neotropical forest and implications for conservation. In Whitmore, T., Chadwick, A., and Sutton, A., editors, *Tropical Rain Forest: Ecology and Management*, pages 25–41. The British Ecological Society, Oxford.
- Hubbell, S. P. and Foster, R. B. (1986). Commonness and rarity in a neotropical forest: implications for tropical tree conservation. In Soule, M., editor, *Conservation biology: the science of scarcity and diversity*, pages 205–231. Sinauer Associates, Sunderland, MA.
- Illian, J., Penttinen, A., Stoyan, H., and Stoyan, D. (2008). *Statistical Analysis and Modelling of Spatial Point Patterns*. John Wiley & Sons.
- Kanaan, M., Taylor, P. C., and Muggleston, M. (2008). Cross-spectral properties of a spatial point-lattice process. *Statistics & Probability Letters*, 78(18):3238–3243.
- Lii, K. and Rosenblatt, M. (2008). Prolate spheroidal spectral estimates. *Statistics & probability letters*, 78(11):1339–1348.
- Matsuda, Y. and Yajima, Y. (2009). Fourier analysis of irregularly spaced data on \mathbb{R}^d . *Journal of the Royal Statistical Society Series B: Statistical Methodology*, 71(1):191–217.
- Miller, K. S. (1980). *Hypothesis testing with complex distributions*. Krieger, Huntington - N.Y.
- Møller, J., Syversveen, A. R., and Waagepetersen, R. P. (1998). Log Gaussian Cox processes. *Scandinavian journal of statistics*, 25(3):451–482.
- Møller, J. and Waagepetersen, R. P. (2003). *Statistical Inference and Simulation for Spatial Point Processes*. CRC press.
- Muggleston, M. A. and Renshaw, E. (1996a). The exploratory analysis of bivariate spatial point patterns using cross-spectra. *Environmetrics*, 7(4):361–377.
- Muggleston, M. A. and Renshaw, E. (1996b). A practical guide to the spectral analysis of spatial point processes. *Computational Statistics & Data Analysis*, 21(1):43–65.
- Neyman, J. and Scott, E. L. (1972). Processes of clustering and applications. *Stochastic point processes*, pages 646–681.
- Percival, D. B. and Walden, A. T. (1993). *Spectral Analysis for Physical Applications*. Cambridge University Press.
- Rajala, T. A., Olhede, S. C., Grainger, J. P., and Murrell, D. J. (2023). What is the Fourier transform of a spatial point process? *IEEE Transactions on Information Theory*, 69(8):5219–5252.
- Renshaw, E. (2002). Two-dimensional spectral analysis for marked point processes. *Biometrical Journal: Journal of Mathematical Methods in Biosciences*, 44(6):718–745.
- Riedel, K. S. and Sidorenko, A. (1995). Minimum bias multiple taper spectral estimation. *IEEE Transactions on Signal Processing*, 43(1):188–195.
- Simons, F. J. and Wang, D. V. (2011). Spatiospectral concentration in the Cartesian plane. *GEM-International Journal on Geomathematics*, 2:1–36.
- Slepian, D. (1983). Some comments on Fourier analysis, uncertainty and modeling. *SIAM review*, 25(3):379–393.
- Slepian, D. and Pollak, H. O. (1961). Prolate spheroidal wave functions, Fourier analysis and uncertainty–i. *Bell System Technical Journal*, 40(1):43–63.
- Thomson, D. (1982). Spectrum estimation and harmonic analysis. *Proceedings of the IEEE*, 70(9):1055–1096.
- Waagepetersen, R., Guan, Y., Jalilian, A., and Mateu, J. (2016). Analysis of multispecies point patterns by using multivariate log-Gaussian Cox processes. *Journal of the Royal Statistical Society: Series C (Applied Statistics)*, 65(1):77–96.
- Walden, A. T. (2000). A unified view of multitaper multivariate spectral estimation. *Biometrika*, 87(4):767–788.
- Whittaker, J. (2009). *Graphical Models in Applied Multivariate Statistics*. Wiley Publishing.
- Yang, J. and Guan, Y. (2024). Fourier analysis of spatial point processes. *arXiv preprint arXiv:2401.06403*.
- Young, W. H. (1912). On the multiplication of successions of Fourier constants. *Proceedings of the Royal Society of London. Series A, Containing Papers of a Mathematical and Physical Character*, 87(596):331–339.
- Zemunik, G., Winter, K., and Turner, B. L. (2020). Toxic effects of soil manganese on tropical trees. *Plant and Soil*, 453:343–354.